Solid Earth, 17, 485–512, 2026
https://doi.org/10.5194/se-17-485-2026
© Author(s) 2026. This work is distributed under
the Creative Commons Attribution 4.0 License.

Solid Earth Open Access EGU

The influence of burial history on physical rock properties: a case study of Lower Jurassic claystones from the Hils and Sack Synclines (Germany)

Raphael Burchartz[1], Timo Seemann[1], Garri Gaus[2,4], Lisa Winhausen[1], Mohammadreza Jalali[1], Brian Mutuma Mbui[2], Sebastian Grohmann[2], Linda Burnaz[2], Marlise Colling Cassel[2], Jochen Erbacher[3], Ralf Littke[2], and Florian Amann[1,4]

[1]Institute of Engineering Geology and Hydrogeology, RWTH-Aachen University, 52064 Aachen, Germany
[2]Institute of Organic Biogeochemistry in Geo-Systems, RWTH-Aachen University, 52064 Aachen, Germany
[3]Federal Institute for Geosciences and Natural Resources, 30655 Hannover, Germany
[4]Fraunhofer Research Institution for Energy Infrastructures and Geotechnologies IEG, 52056 Aachen, Germany

Correspondence: Raphael Burchartz (burchartz@lih.rwth-aachen.de)

Received: 7 February 2025 – Discussion started: 25 March 2025
Revised: 12 February 2026 – Accepted: 2 March 2026 – Published: 18 March 2026

Abstract. The search for a suitable host rock for the deep geological disposal of high-level radioactive waste is a major societal challenge of our time. In Germany, clay-bearing formations are under investigation to potentially host a repository for high-level radioactive waste (alongside rock salt and crystalline rock). Their intrinsic properties such as low permeability, self-sealing efficiency with respect to fractures, and sorption capacity provide promising conditions for long-term waste containment. However, these properties are dependent on numerous factors such as mineralogical composition, temperature and stress conditions, and water content. Among these factors, the burial history and thus compaction affect mineralogy, porosity, permeability, and mechanical properties. Within the framework of the MATURITY project, the impact of the burial history on these properties is investigated based on a combination of different laboratory and field methods. For this purpose, a Lower Jurassic claystone formation (the Amaltheenton-Formation, Fm) which was subjected to variable maximum depth and subsequent uplift during its burial history was chosen as target formation. At five locations, in the margin area of the Lower Saxony Basin (Germany) shallow boreholes were drilled through the formation where varying degrees of maturation indicate substantial differences in maximum burial depth.

In this contribution, we present the first results of initial project steps that show (a) a similar clay-dominated mineralogical composition of the Amaltheenton-Fm across the borehole locations, (b) an increase of max. burial temperatures (83–169 °C) over a lateral distance of ∼ 50 km within the investigation area, (c) a gradual increase in bulk density accompanied by a reduction in porosity and permeability for normally-compacted Amaltheenton-Fm sequences along increasing max. burial temperatures, (d) a reverse trend of those parameters for a potentially undercompacted Amaltheenton-Fm sequence, and (e) hydraulic conductivity determined from in-situ hydraulic tests that significantly differs from laboratory derived equivalents and span two orders of magnitude (10^{-5} to 10^{-7} m s^{-1}).

1 Introduction

Claystones are considered as potential host rocks for the long-term disposal of high-level radioactive waste (HLW) in many countries. Famous examples of European HLW host rock candidates include the Opalinus Clay (OPA; Switzerland), the Boom Clay (Belgium), and the Callovo–Oxfordian argillite (COx, France) (Delage et al., 2010; Norris, 2017). Their suitability to act as natural barriers is mainly due to favorable properties, such as very low permeability (down to 10^{-21} m^2), preventing significant focused fluid flow and related advective mass transport of radionuclides in aqueous

solutions (OECD and NEA, 2022; Fisher et al., 2023). Additionally, their nuclide sorption capacity and self-sealing behavior mitigate the risk of radionuclide migration into the environment (Bastiaens et al., 2007; OECD and Nuclear Energy Agency, 2022). However, there are numerous factors influencing these key properties and the related sealing integrity of potential host rock formations, posing considerable complexity to site selection procedures. Among other factors such as mineralogical composition and pore water salinity (Bonin, 1998; Dewhurst et al., 1999; Carcione et al., 2019), the burial history exerts important controls on porosity, bulk density, permeability, and mechanical properties such as strength and elasticity (Jones and Addis, 1985; Bjørlykke and Høeg, 1997; Dewhurst et al., 1998; Czerewko and Cripps, 2006; Cripps and Czerewko, 2017; Ewy et al., 2020). Burial-related alterations in claystones, are mainly attributed to compaction as a consequence of changing in-situ stress and temperature conditions (Fig. 1) (Aplin and Yang, 1995; Bjørlykke, 2006; Cripps and Czerewko, 2017; Ewy et al., 2020; Fisher et al., 2023). Further alteration of those properties might additionally be induced by processes such as uplift, erosion, and isostatic rebounding during the course of the burial history (Fink et al., 2019; Mazurek et al., 2023).

One of the fundamental changes in claystones associated with progressive burial is the gradual reduction of porosity and bulk volume, accompanied by an increase in density and elasticity (Athy, 1930; Aplin and Yang, 1995; Aplin et al., 2006; Ewy et al., 2020; Fisher et al., 2023). The reduction of porosity in claystones is typically a result of the combined effects of mechanical and chemical compaction, such as the precipitation of carbonaceous or siliceous mineral phases (Jones and Addis, 1984; Addis and Jones, 1985; Jones and Addis, 1985; Broichhausen et al., 2005; Bjørlykke, 2006; Armitage et al., 2010; Ewy et al., 2020). In response to the increase of effective in-situ stress during burial, mechanical compaction controls dewatering processes, pore evolution (void reduction), and particle reorientation, serving as the dominant diagenetic mechanism at relatively shallow depths (< 2 km) and low temperatures (< 70 °C) (Aplin and Yang, 1995; Bjørlykke, 1998; Peltonen et al., 2009; Cripps and Czerewko, 2017). Further, porosity reduction is usually associated with chemical compaction such as mineral cementation and clay mineral reactions occurring during deeper burial and higher related temperatures (> 70 °C) (Bjørlykke, 1998). One of the most important diagenetic clay mineral reactions driven by temperature changes is the progressive transformation of smectite into thermally more stable illite, occurring through an intermediate mixed-layer stage that forms illite/smectite (I/S) mixed-layers (Pollastro, 1993; Berthonneau et al., 2017). This process is commonly referred to as illitization and invokes, besides porosity reduction, dehydration processes, reduced swelling potential, changes in the cation exchange capacity (CEC) and grain sizes (Ohazuruike and Lee, 2023). However, porosity reduction during burial may be impeded by overpressure generation as a result of compaction disequilibrium (undercompaction), hydrocarbon generation, or clay diagenetic processes such as illitization, potentially leading to fracturing processes and fracture-related fluid flow, thus impairing the rock's barrier function (Eaton, 1975; Bowers, 1995; Swarbrick and Osborne, 1998; Hart et al., 2023). Another potential deviation from the general porosity–depth trend may result from early cementation during shallow burial, where chemical lithification occurs prior to significant mechanical compaction (Corkum and Martin, 2007). This process has been increasingly recognized in studies of mudstones and claystones from unconventional resource settings, where early diagenetic cementation can "lock in" porosity and lead to complex, non-monotonic porosity–depth relationships (Aplin and Macquaker, 2011; Minisini et al., 2025).

As clay muds are compacted to lower porosity claystones, permeability can decrease by six or more orders of magnitude (down to 10^{-23} m^2), improving their barrier function in HLW disposal (Neuzil, 2019). Quantification and characterization of claystone permeability have long been recognized as a challenging, time-consuming task (Neuzil, 1994, 2019). A fundamental challenge when quantifying permeability lies in the strong scale dependency (Neuzil, 1994, 2019; Van Der Kamp, 2001). Permeability measurements on smaller-sized low-permeable rocks tend to deliver a measure of the unfractured matrix permeability, while secondary structures such as transmissive fractures remain neglected, even though fractures or other heterogeneities can control the larger-scale hydraulic behaviour (Neuzil, 1994; Van Der Kamp, 2001). Therefore, differences between the matrix and effective permeability might differ by orders of magnitude (Van Der Kamp, 2001), and scale dependencies have to be considered during repository planning.

Shallowly buried, soft, soil-like clays and claystones such as Boom Clay in Belgium hold advantages in terms of sealing integrity as the ductile behaviour of the material prevents larger brittle fractures to form easily. In addition, self-sealing as a result of clay mineral swelling can play a crucial role if the formation is not already saturated and/or if a pore fluid change to lower-ionic strength is at play, as it allows for fracture closure within short time spans (Bastiaens et al., 2007). With progressive induration along deeper burial, claystones become more brittle promoting fracturing and potentially enhancing preferential fluid pathways, e.g., in an excavation damage zone (Neuzil, 1994; Bossart et al., 2002, 2004). Fracture self-sealing due to swelling might be effective but occurs over longer time-spans (Bastiaens et al., 2007; Bock et al., 2010; Guglielmi et al., 2025).

Relatively low rock strength of claystones and strength anisotropy due to their bedded structure may hold considerable influence on the construction of underground facilities (Blümling et al., 2007; Wild and Amann, 2018a). Various experimental studies demonstrated that the mechanical behavior of claystones mainly depends on (a) the mineralogical composition, (b) the porosity and water saturation, and

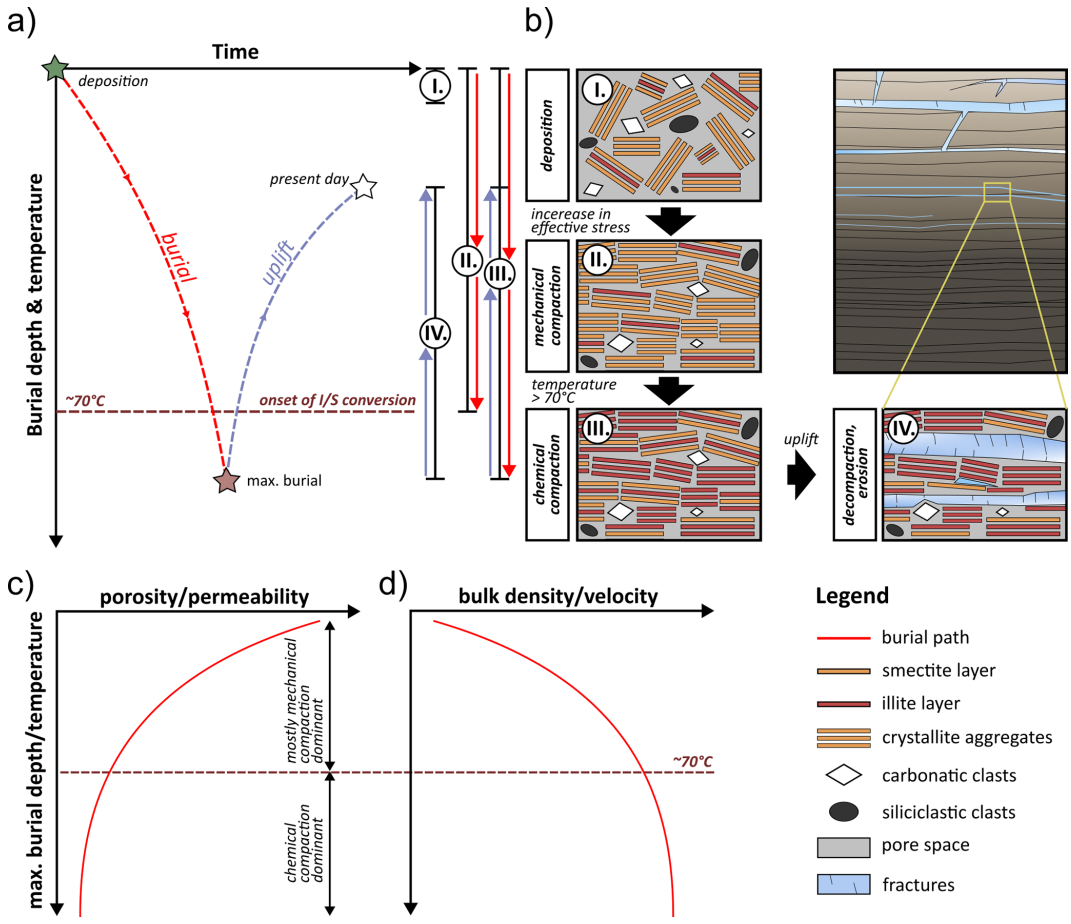

Figure 1. Simplified and condensed alterations in claystones induced by changing in-situ stress and temperature conditions along their burial history: **(a)** the general burial history of claystones. Roman numbers represent essential processes along the burial history of claystones with I. = deposition, II. = mechanical compaction, III. = chemical compaction, and IV. = uplift (modified after: Lehocki and Avseth, 2021). The range bars and colored arrows mark ranges along the burial history in which the respective process contributes to alterations within the claystones. While mechanical compaction is only effective during burial, chemical compaction remains also active during uplift; **(b)** alterations in claystones induced by the processes I., II., III., and IV. During deposition, clays show a random assemblage of crystallite aggregates. The porosity dependents on detrital clay composition and assemblage architecture. An increase in effective in-situ stress will lead to realignment and close packing of aggregates, reduced pore space, expulsion of pore water. Chemical compaction becomes the dominant compaction process when temperatures reach > 70 °C. Dissolution, cementation, and mineral reactions such as illite-smectite conversion will lead to further loss of porosity. Uplift will lead to decompaction, erosion, and fracturing (mainly along bedding); **(c)** and **(d)** show burial related trends in different claystone properties **(c)** modified after Bjørlykke, 1998).

(c) pressure and temperature conditions (Ibanez and Kronenberg, 1993; Aplin and Macquaker, 2011; Sone and Zoback, 2013; Rybacki et al., 2015; Amann et al., 2017; Busch et al., 2017; Cripps and Czerewko, 2017; Rutter et al., 2017; Wild and Amann, 2018a, b; Winhausen et al., 2022, 2023). At the formation/basin scale, the mechanical behavior is therefore dependent on (a) the depositional environment and resulting mineralogical composition, and (b) the burial history with related pressure and temperature conditions, systematically altering the physical and chemical properties from the moment of deposition. In general, the mechanical behavior shows a transition from soil-like ductile to rock-like brittle behavior with increasing burial depth due to various diagenetic mechanisms, such as (i) closer grain-to-grain bonding of clay grains with decreasing porosity and (ii) the formation of cementing minerals, like carbonates or silicates (Ewy et al., 2020).

Following maximum burial, uplift processes such as exhumation, erosion, and isostatic rebound, lead to stress relief, which typically promotes the formation of discontinuities or fracturing (Czerewko and Cripps, 2006). This degradation process can result in the development of a decompaction zone (Fig. 1b), where porosity, permeability, mineralogy, and pore water characteristics are markedly altered. Such zones might reach several decametres of depth below surface (Hekel, 1994; Vogt et al., 2017; Crisci et al., 2019; Mazurek et al., 2023). In addition, the reduction in effective

stress during uplift leads to overconsolidation (present effective stress < past effective stress) of the formation, which is associated with an increase in shear strength and brittleness (Wagner, 2013; Winhausen et al., 2022).

Along the site-selection process the commonly used transfer of geoscientific data (Mazurek et al., 2008) need to account for the mutual and complex (inter-)dependencies between claystone properties and their burial history as they hold the potential of influencing mechanical, hydraulic, and sorption characteristics even within the same formation. Hence, systematic studies on the depth- and temperature-dependent progression of these changes are needed that help to quantify the induced alterations and benefit data transfer across sites. However, to present day such studies remain scarce, as obtaining representative samples across different stages of diagenetic maturity typically requires costly and logistically demanding deep drilling campaigns. The MATURITY project, launched in 2022, seeks to fill this gap through a field-to-lab-scale research initiative carried out within the Amaltheenton-Fm, a Lower Jurassic (Late Pliensbachian) organic matter-lean marine claystone.

1.1 MATURITY project outline

The overall objectives of the MATURITY project can be delineated as follows:

- Comprehensive and systematic characterization of the mechanical, sedimentological, and hydraulic properties of Pliensbachian claystones that are considered as potential host rock in the German siting approach.
- Assessment of correlations among sedimentological, hydraulic, geomechanical, and petrophysical properties and their dependence on thermal maturity, with the aim of establishing a basis for the transferability of results to potential future repository sites.
- Investigation of scale-dependent behavior, focusing on the characterization of large-scale hydraulic and elastic properties.
- Development of an in-situ long-term observatory to enable sustained monitoring of long-term stability and to provide a framework for subsequent studies addressing the quantification of transport properties at the rock mass scale.

These objectives are addressed based on a comprehensive catalogue of field and laboratory methods applied within shallow boreholes or on drill-core samples obtained during the drilling process. The choice of shallow investigation depth (< 100 m below surface) avoids the need for mining permits under German regulations and therefore simplifies permitting and benefits cost efficient and rapid drilling procedures. The general project approach is schematically shown in Fig. 2.

To study the explicit influence of burial history on physical claystone properties, the investigated rock sequences should ideally exhibit a high variability in thermal maturity while other controlling factors, particularly mineralogical composition, remain similar. This ensures that variability in the observed rock properties is predominantly controlled by burial-related alteration processes. Previous studies (i.e. Koch and Arnemann, 1975; Littke et al., 1988; Mackenzie et al., 1988; Bruns et al., 2016) document pronounced thermal maturity variations over short distances within parts of the Lower Saxony Basin (LSB), Germany, making this region particularly suitable for the MATURITY project. Although several lithostratigraphic units in the area, including the Amaltheenton-Fm and the Opalinuston-Fm/Jurensismergel-Fm, are evaluated as potential sub-areas in the German siting process (Fig. 3), the Amaltheenton-Fm was selected as the primary target formation of this study. The Opalinuston-Fm/Jurensismergel-Fm locally exhibits deformation related to degassing of the underlying Posidonienschiefer-Fm and occurs in a hanging-wall position closer to the surface, increasing the likelihood of weathering-related alteration.

1.2 Objectives of this study

In this contribution, we set the outline for a series of detailed parameter studies conducted in the framework of the MATURITY project. Collectively, these studies are designed to improve our understanding of how burial history alters claystone properties, facilitating the data transfer across claystone siting regions in Germany. The present study addresses four substantial aims:

- report on first measurement results of the MATURITY project and on how and where they were obtained,
- comparison of borehole and laboratory derived measurement results,
- comparison of max. burial values from VRr % and 3D modelling,
- discussion of the influence of max. burial on physical rock properties.

2 Study area

This section introduces the geological and structural setting of the Hils and Sack Synclines. In addition, it summarizes previous investigations that document the pronounced burial depth and maturity gradients in the region, which form the basis for the site selection and result interpretation of the present study.

2.1 Geological outline

The Hils and the adjacent Sack Syncline structures are located in the southern part of Lower Saxony (Germany), ap-

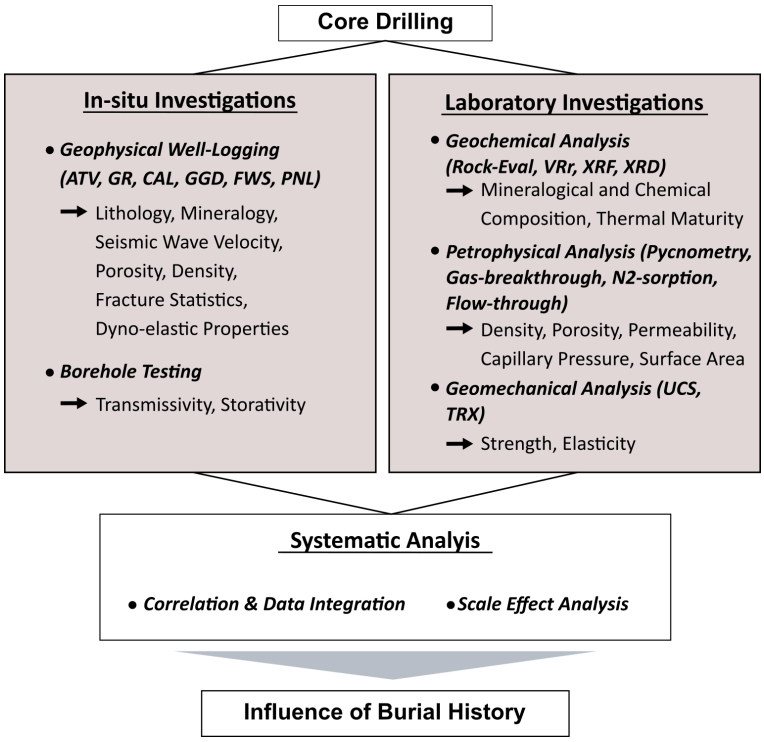

Figure 2. MATURITY project overview with the principal project objectives and general investigation approach. ATV = Acoustic borehole televiewer, GR = Gamma-ray, CAL = Caliper log, GGD = Gamma-gamma-density, FWS = Fullwave Sonic log, PNL = Pulsed-neutron lifetime log, VRr = Vitrinite reflectance, XRF = X-ray fluorescence, XRD = X-ray diffraction, UCS = Uniaxial compressive strength test, TRX = Triaxial compressive strength test.

proximately 50 km south of Hanover. Both are assigned to the southeastern margin area of the Lower Saxony Basin (LSB), which represents an E-W striking, highly differentiated Meso-Cenozoic basin system, which is, in turn, part of the Central European Basin System (CEBS) (Van Wees et al., 2000; Adriasola Muñoz, 2007; Maystrenko et al., 2008; Castro-Vera et al., 2024). The CEBS formed initially as a result of Late Carboniferous to Early Permian igneous activity, faulting and lithosphere subsidence (Van Wees et al., 2000; Adriasola Muñoz, 2007; Burnaz et al., 2024). During this phase, the deposition of terrestrial sediments was dominant. From the latest Permian to the Late Triassic, the depositional setting was terrigenous to shallow-marine. A progressive transgression from the onset of the Jurassic period led to marine sedimentation, which in the Early Jurassic (Sinemurian to Toarcian) and the lower Middle Jurassic (Aalenian to Bajocian) resulted in the deposition of argillaceous sequences with variable carbonate content. During the Toarcian, anoxic-euxinic conditions led to the formation of the organic matter-rich Posidonienschiefer-Fm in a marginal marine environmental setting (Stahl, 1992; Maystrenko et al., 2008; Hooker et al., 2020). During the Middle Jurassic, repetitive sea level fluctuations (transgression–regression cycles) led to sandy interlayers within marine claystones. The clastic influx ceased during the Callovian and the Oxfordian is characterized by open marine claystone successions with interlayered carbonate sequences, especially in the upper Oxfordian (Stollhofen et al., 2008; Bruns et al., 2013). Late Jurassic–Early Cretaceous rifting processes initiated the formation of the LSB, resulting in its rapid subsidence while the adjacent blocks, e.g., the Rheinish Massif in the south and the Pompeckj Block in the north, experienced strong uplift (Kockel et al., 1994; Senglaub et al., 2005). Sedimentation within the LSB remained predominantly shallow marine with terrestrial sediments being confined to the transition between the uppermost Jurassic and lowermost Cretaceous (Münder-Formation and Bückeberg-Group, Purbeck and Wealden Facies) (Stollhofen et al., 2008; Bruns et al., 2013). Inversion tectonics, beginning in the Upper Cretaceous (Coniacian-Santonian), triggered the structural uplift of the LSB and with it that of the Hils and the Sack Syncline (Stahl, 1992; Voigt et al., 2021). Existing normal faults were reactivated and transformed into steep thrust and reverse faults (Stahl, 1992; Petmecky et al., 1999; Baldschuhn and Kockel, 1998; Senglaub et al., 2005). Later, the individual inversion structures underwent deep erosion beneath the Campanian unconformity and once more before the Late Paleocene transgression (Stahl, 1992). Figure 4 summarizes the principal tecto-sedimentological conditions and resulting geological structures and sequences. For more detailed infor-

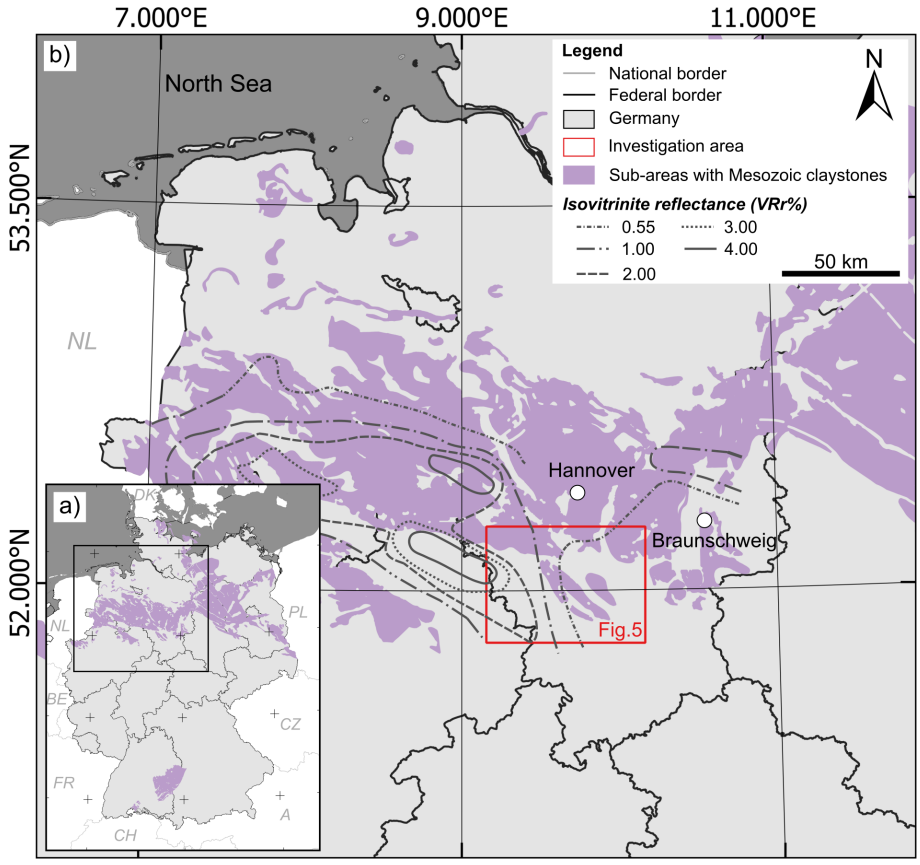

Figure 3. **(a)** Map of Mesozoic claystone sub-areas in northwestern Germany identified by BGE in accordance with §13 StandAG (modified after: BGE, 2020); **(b)** overview map of Lower Saxony with indication of the investigation area and isovitrinite reflectance contour lines (Isovitrinite reflectance modified after: Mackenzie et al., 1988; Klaver et al., 2012).

mation on the geodynamic and sedimentological evolution of the CEBS and the LSB the reader is referred to (Betz et al., 1987; Van Wees et al., 2000; Adriasola Muñoz, 2007; Bachmann et al., 2008; Bruns et al., 2013).

The lithostratigraphic terms used here correspond to the definition of the stratigraphic database Litholex compiled by the German Stratigraphic Commission. Consequently, German terms are not translated and consistently used as proper terms (litholex.bgr.de).

The Hils and Sack Synclines exhibit a lithological relief inversion towards the syncline center, with the Lower to Middle Jurassic claystone sequences of the Pliensbachian to Aalenian dipping from the syncline margins towards the center at angles between 5 and 30° (Schmitz, 1980; Stahl, 1992; Wiese and Arp, 2013; Heunisch et al., 2018). The syncline centers are characterized by sequences of Upper Jurassic and Lower Cretaceous sedimentary rocks, primarily consisting of limestones, marlstones, and sandstones, which form the geomorphological elevations of the Hils and Sack, and constitute part of the Weser–Leine Uplands. Wiese and Arp (2013) provide detailed litho-stratigraphic descriptions of the Hils and Sack Syncline area. The geological map and cross-section in Fig. 5 outline the present-day local geological conditions of the Hils and Sack syncline. Isovitrinite lines, compiled from former studies of the region (Mackenzie et al., 1988; Castro-Vera et al., 2024), show the increasing thermal maturation trend from SE towards NW, and emphasize the strongly variable burial conditions within the investigated area.

2.2 Previous studies on the burial and maturity gradients in the Hils and Sack Syncline region

Since the late 1980s, the area of the Hils Syncline has been investigated primarily focusing on the hydrocarbon generation potential of the Posidonienschiefer-Fm, which represents western Europe's most important petroleum source rock (Littke et al., 1988; Rullkötter et al., 1988). Several shallow boreholes (approximately 60–80 m of depth) were drilled along the southern margin of the Hils Syncline and penetrated a succession of Lower (Pliensbachian) to Middle (Aalenian) Jurassic claystones (Rullkötter et al., 1988). Based on vitrinite reflectance values (VRr), the thermal maturation sequence increases from southeast to northwest from 0.48 to 1.45 VRr % (Littke and Rullkötter, 1987; Littke et al., 1991). This trend has been repeatedly reaffirmed by several

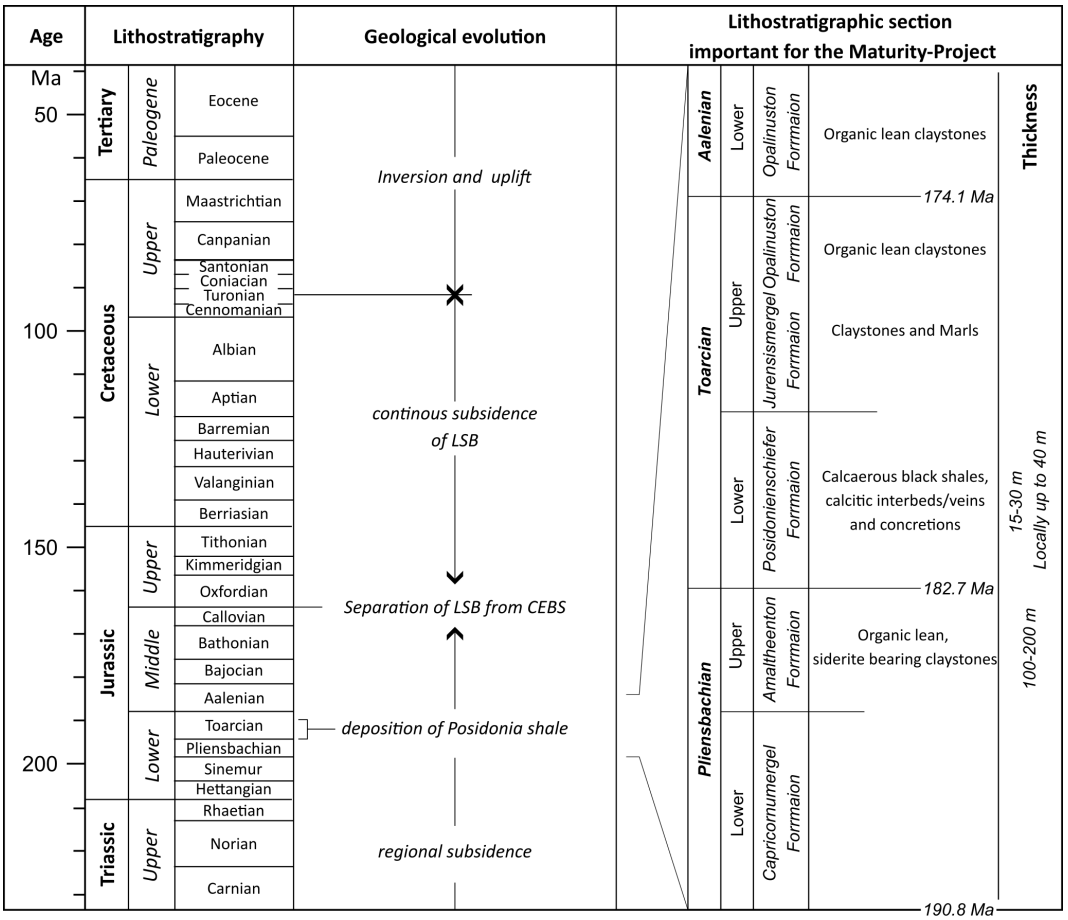

Figure 4. Lithostratigraphic overview and geologic evolution of the LSB (modified after LBEG Stratigraphische Kommission, Castro-Vera et al., 2024).

studies (see Bernard et al., 2012; Klaver et al., 2012; Ghanizadeh et al., 2014). While early studies assumed thermal maturation caused by a deep-seated mafic intrusion, younger studies (Petmecky et al., 1999; Senglaub et al., 2005) more plausibly evidenced the maturity differences caused by differential burial. Recent investigations confirmed the consistent depositional environments during the Pliensbachian (Burnaz et al., 2024; Wijesinghe et al., 2025) and local variations in burial and temperature history (Fink et al., 2019; Castro-Vera et al., 2024) resulting in mineralogically similar clay-dominated sequences with different thermal maturities.

Mann (1987) documented a steady decrease in mean pore radii of Posidonienschiefer-Fm samples from 60 to 2.2 nm between the Wenzen (Wen) and Harderode (Har) boreholes (Fig. 5). Slightly higher values of 3.2 nm were determined for samples from the Haddessen (Had) borehole. Correspondingly, average porosities showed a gradual decrease with values ranging from 20 % in Wenzen to partly < 5 % in Harderode. A slight increase in porosity was observed between the Har and the Had borehole, where porosities were measured at > 8 %. The specific surface area was found to decrease from 18 to 0.5 $m^2 g^{-1}$ (Mann, 1987). These results were corroborated by similar findings in more recent studies, all showing a minimum porosity at the intermediate maturity stage (oil-window, Harderode) (see Klaver et al., 2012; Gasparik et al., 2014; Ghanizadeh et al., 2014; Rybacki et al., 2015; Grathoff et al., 2016; Mathia et al., 2016; Mohnhoff et al., 2016). The initial decrease in porosity is interpreted as a combined effect of enhanced cementation and compaction during burial, while the increase from intermediate-mature samples (0.91 VRr %) to post-mature samples (1.52 VRr %, gas-window, Haddessen) is seen as result of secondary porosity evolution in the residual organic matter (Klaver et al., 2012; Mathia et al., 2016; Mohnhoff et al., 2016). Permeabilities were found to follow a similar trend with a range between 10^{-17} to 10^{-22} m^2 and a minimum permeability in the intermediate maturity stage (Ghanizadeh et al., 2014; Grathoff et al., 2016; Mohnhoff et al., 2016). Rybacki et al. (2015) report on a peak in uniaxial compressive strength (UCS) of Posidonienshiefer-Fm specimen from the Harderode borehole (0.9 VRr %) and lower UCS values measured on specimen from boreholes Wickensen (0.6 VRr %)

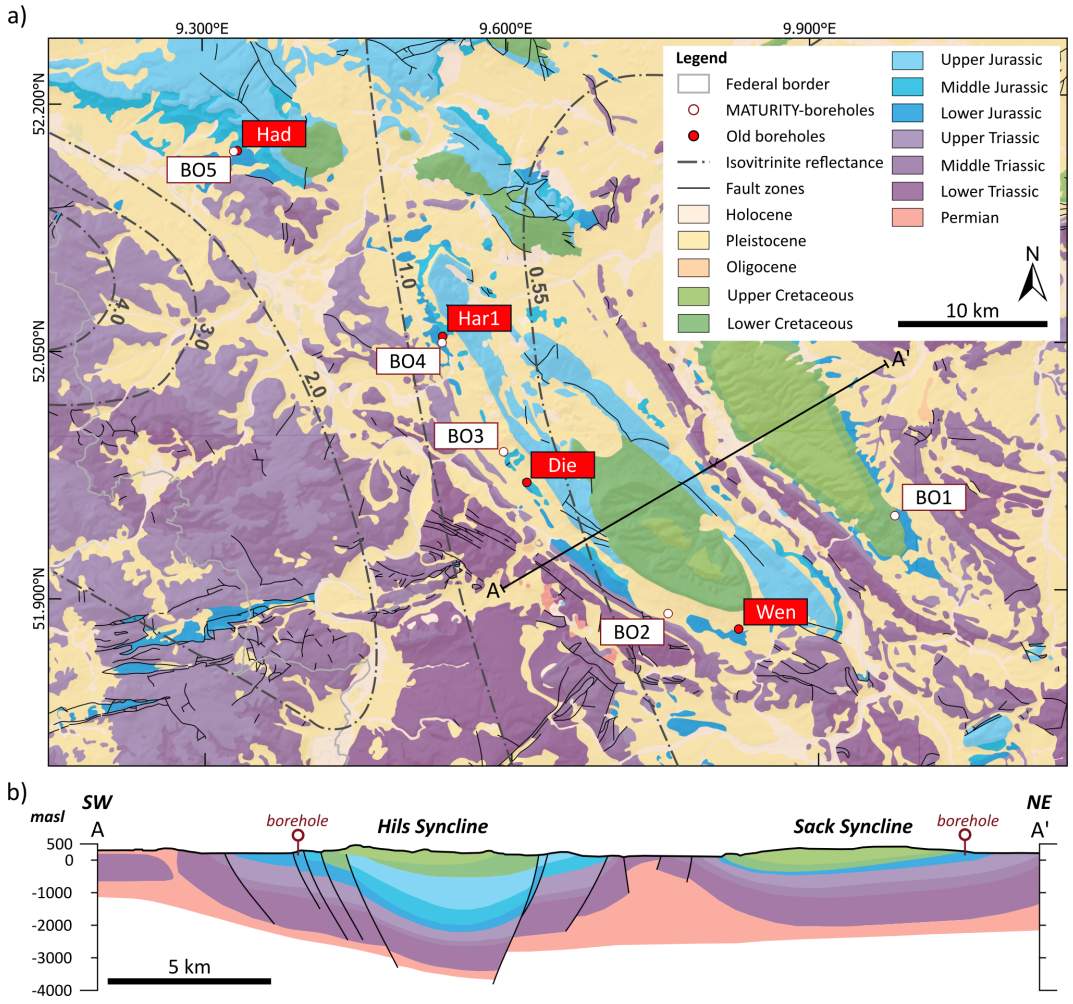

Figure 5. (a) Geological Map (NIBIS® Kartenserver, 2014) with indication of borehole locations from previous studies and the MATURITY project **(b)** cross section of the Hils and Sack Syncline with approximate indication of borehole locations. Isovitrinite reflectance lines are added based on: Mackenzie et al. (1988); Castro-Vera et al. (2024). The geological cross section was modified after Jordan et al. (1989) and Wiese and Arp (2013).

and Haddessen (1.3 VRr %). Similarly, triaxial tests at 50 and 100 MPa confining pressure yielded shear strength values in the order Har > Had > Wic. Mann and Müller (1988) showed, among other findings, a trend of increasing density from gamma-gamma (GGD) and neutron density data across the boreholes Wen, Diel, Had, corresponding to increasing thermal maturity quantified by the maximum temperature during pyrolytic degradation (T_{max}). It should be emphasized that these data refer to the Toarcian Posidonienschiefer-Fm not the Amaltheenton-Fm which is the focus of the present study. The Posidonienschiefer-Fm is not considered as a potential host rock for radioactive waste disposal due to its distinctive composition, characterized by a high carbonate and organic matter content, thus holding the potential for microbial activity, enhanced chemical reactivity, and oil and gas generation (Rullkötter et al., 1988). However, due to their stratigraphic proximity and overlapping burial and thermal histories, insights from the Posidonienschiefer are valuable for understanding the expected maturity-related trends in the underlying Amaltheenton-Fm.

In a pre-study towards the initiation of the MATURITY project, Gaus et al. (2022) investigated the petrophysical (porosity, permeability) and mechanical (uniaxial compressive strength) characteristics of core materials from the 1980's drilling campaign. They were the first to focus on the organic-lean Amaltheenton-Fm. In their approach, thermal maturities, derived from VRr values, were taken as a proxy for burial depths and related temperatures, indicating maximum burial depths between 1300 and 3600 m. Their results align with the previous studies on the organic-rich Posidonienschiefer-Fm, revealing an initial decrease of porosity and permeability until the intermediate maturation stage (or related burial depth of approximately 2650 m in Harderode) from 18 % to 5 % and 2.7 to 0.21×10^{-21} m^2,

respectively. A slight increase in those properties was observed for over-mature samples from the Haddessen borehole (or related burial depth of 3660 m). Uniaxial compressive strength data showed a reverse trend, increasing from 25 to 40 MPa at burial depths ranging from 1300 to 2650 m, whereas the sample from deeper burial of 3660 m yielded a UCS value of 37 MPa. The latter observation contradicts the general burial trend. Possible explanations are given by Castro-Vera et al. (2024), who published a 3D basin model based on data from newly drilled boreholes during the MATURITY project and the Wenzen borehole. Following this model, a gradual increase in maximum burial depth from 1400 m (BO2.0) to 3300 m (BO5.0) is responsible for stated trends in thermal maturity. However, localized overpressure generation due to undercompaction in the Amaltheenton-Fm and overpressure propagation originated in the overlying Posidonienschiefer-Fm due to gas generation likely explains the stated trends of decreasing density and increasing porosity within the Amaltheenton- Fm below 2440 m (Gaus et al., 2022; Castro-Vera et al., 2024).

It is acknowledged that the measurements performed on core material recovered in the 1980s must be interpreted with caution due to possible alterations from long-term storage, including drying, oxidation, and fracturing. However, Gaus et al. (2022) critically assessed these limitations and argued that despite potential alteration, the measured petrophysical and mechanical properties likely still reflect representative matrix characteristics. Supporting evidence includes the preservation of pyrite, absence of gypsum formation, consistent bulk density values with comparable claystones, and lack of macroscopic fractures after drying, suggesting limited mineralogical or structural degradation of the cores.

3 Methods

For this study, an initial series of in-situ and laboratory investigations was conducted. The applied methodologies are briefly outlined in the following Sect. 3.1 Borehole selection and drilling processes.

3.1 Borehole selection and drilling processes

The basis for the proposed investigations on the Amaltheenton-Fm are six newly drilled boreholes within the western flank of the Hils Syncline and two boreholes on the south-eastern margin of the Sack Syncline. The selection of the borehole locations is based on (a) the findings of previous studies stating an increasing trend of thermal maturity from southeast to northwest, and (b) structural field data (dip and dip direction) measured in outcrops and taken from old borehole data to estimate the upper boundary of the Amaltheenton-Fm, aiming to minimize the influence of surface weathering.

In total, eight new boreholes at five different locations (BO1, BO2, BO3, BO4, BO5) were drilled in the scope of the MATURITY project from July 2022 to October 2023 within the target area (Fig. 5). Three locations (BO1, BO3, and BO5) were equipped with doublet boreholes with a horizontal spacing of approximately 5 m. All boreholes were fully cored in stable rock sequences using a triple tube core barrel and a polymer-based drilling fluid (Pure-Bore©) to prevent clay mineral swelling. Permanent, cemented metal casings stabilized unstable rock and soil sequences. An overview of the individual borehole locations and specifications is given in Table 1.

3.2 Geophysical borehole investigations

Geophysical wireline logging was carried out in the boreholes right after the drilling process. The applied logging methods comprise natural and spectral gamma-ray spectroscopy (NGR/SGR), acoustic borehole televiewer (ATV), resistivity, full-wave sonic (FWS), gamma-gamma-density (GGD), pulsed-neutron lifetime (PNL), temperature, and caliper (CAL) logging. While GR, ATV, FWS, and CAL logs were recorded in all boreholes, GGD and PNL logging was only conducted in the boreholes BO1.1, BO3.0, and BO5.0. Because of borehole wall instability, borehole BO1.0 could only be logged with a temperature probe and integrated natural gamma-ray tool, while borehole BO2.0 could only be logged in an open borehole section between the casing (47 m) and a borehole blockage at 87 m of depth. In this contribution, selected logging results mainly from the Amaltheenton-Fm will be presented, providing a first in-situ characterization of different formation properties.

Spectrometric Thorium/Potassium (Th/K) and Thorium/Uranium (Th/U) ratios were derived from the SGR logging signals. The Th/K cross-plot, proposed by Quirein et al. (1982) and repetitively modified by Schlumberger (2009), is a widely used technique in spectral gamma-ray log interpretation for identifying clay mineral assemblages (Rider, 2000; Klaja and Dudek, 2016). This method leverages the fact that different clay minerals have characteristic ratios of thorium to potassium due to their distinct geochemical nature and formation conditions, potentially providing knowledge of mineralogical composition (Weaver and Pollard, 1973; Fertl and Chilingarian, 1990; Rider, 2000; Klaja and Dudek, 2016; Gama and Schwark, 2022). In claystones, a low Th/K ratio ($Th/K < 4$) is associated with a dominance in illite, mica, glauconite, or feldspar minerals. In contrast, higher Th/K ratios ($Th/K > 6$) indicate an enrichment in kaolinite and/or heavy minerals (Rider, 2000; Gama and Schwark, 2022). The ratio between thorium and uranium, on the other hand, serves as an indicator of the depositional environmental, weathering, and redox conditions (Adams and Weaver, 1958; Klaja and Dudek, 2016). In a first approximation, we use these empirical correlations to give a general idea of the clay mineralogical composition of the Amaltheenton-Fm, as well as

Table 1. Summary of borehole information. m a.s.l. = metres above sea level, m b.g.s. = metres below ground surface.

Location	Boreholes	Depth (m)	Elevation (m a.s.l.)	Borehole Diameter (mm)	Amaltheenton-Fm top depth (m b.g.s.)
BO1	BO1.0	92.5	252	146	65
	BO1.1	94.0			65
BO2	BO2.0	99.0	227	146	32
BO3	BO3.0	102.0	156	146	74
	BO3.1	101.0			75
BO4	BO4.0	95.0	168	146	6
BO5	BO5.0	98.8	119	146	37
	BO5.1	98.5			38

compare the Amaltheenton-Fm at the individual locations. Bulk densities (ρ_{bulk}) were sampled from GGD logging signals. Porosities were derived by applying:

$$\phi_{\text{dyn}} = \frac{\rho_{\text{matrix}} - \rho_{\text{bulk}}}{\rho_{\text{matrix}} - \rho_{\text{fluid}}} \quad (1)$$

with ϕ_{dyn} being the in-situ porosity derived from the logging signal. Porosity calculations were evaluated under the assumption of a constant matrix density (grain density) (ρ_{matrix}) of $2.7\,\text{g}\,\text{cm}^{-3}$ and a fluid density (ρ_{fluid}) of $1.0\,\text{g}\,\text{cm}^{-3}$.

3.3 Hydrogeological borehole investigations

Hydraulic borehole tests were conducted using either a mobile straddle double packer system (BO2.0 and BO4.0) at various borehole depths or fixed Standpipe Double Packer Systems (SPDP) with one isolated hydraulic interval. A first test series of slug withdrawal (SW) tests was conducted in boreholes BO1.0, BO2.0, BO3.1, and BO4.0. For the evaluation of hydraulic parameters (transmissivity, hydraulic conductivity) and corresponding flow dimensions, the pressure over time test data were analyzed using the n-dimensional Statistical Inverse Graphical Hydraulic Test Simulator, nSIGHTS (Roberts, 2006).

In-situ long-term hydraulic observations aiming at time-dependent quantification of flow and transport properties within the Amaltheenton-Fm are conducted by establishing borehole-based investigation systems. For this purpose, the doublet boreholes at the locations BO1, BO3, and BO5 were equipped with Standpipe Double Packer Systems (SPDP), schematically shown in Fig. 6. The installed systems consist of:

- Two inflatable straddle packers for the hydraulic isolation of borehole sections (Fig. 6c). Packers were inflated to 3 MPa inside the boreholes by injecting water. The interval between both packers is 5 m long and contains five 15 µm sinter metal filter elements of 1 m length each (Fig. 6c).
- Stainless steel tubing pipes with space for two standpipes and an operation line for packer lines.
- Two standpipes, which provide access to the interval.
  - *Standpipe 1* (SP1) allows the execution of hydraulic borehole tests (injection or withdrawal). SP1 is closed at the lower end with a pneumatic downhole valve.
  - *Standpipe 2* (SP2) is equipped with a pressure-temperature sensor (P/T) at the lower end, constantly measuring the interval pressure and temperature. It is sealed with a mini-packer on top of the P/T sensor.
- Caverns of 2 m depth and 1.2 m diameter, on the top of each borehole for data acquisition and system operation equipment (Fig. 6b and d) containing:
  - Flowboard with manometers, valves, and pressure-line connections for pressure regulation of packers.
  - Data logger for constant data acquisition.
  - Nitrogen tanks for pressure stabilization of packers.
  - Upper end of the steel tubing pipes with access to SP1 and SP2.

The systems installed allow hydraulic testing of isolated intervals through the injection or extraction of fluid into or from the interval. Continuous recording of pressure and temperature conditions via the P/T sensor installed in SP2 enables monitoring the long-term evolution of the interval pressure. Through numerical analysis, this data can be analyzed to derive information about permeability, storage capacity, and pore pressure conditions. Interference tests between the adjacent boreholes are designed to facilitate the quantification of these parameters beyond the borehole-influenced zone, and changes between fracture- and matrix-dominated flow. Furthermore, the extraction of water from the test interval (via SP1) provides the opportunity to sample and analyze

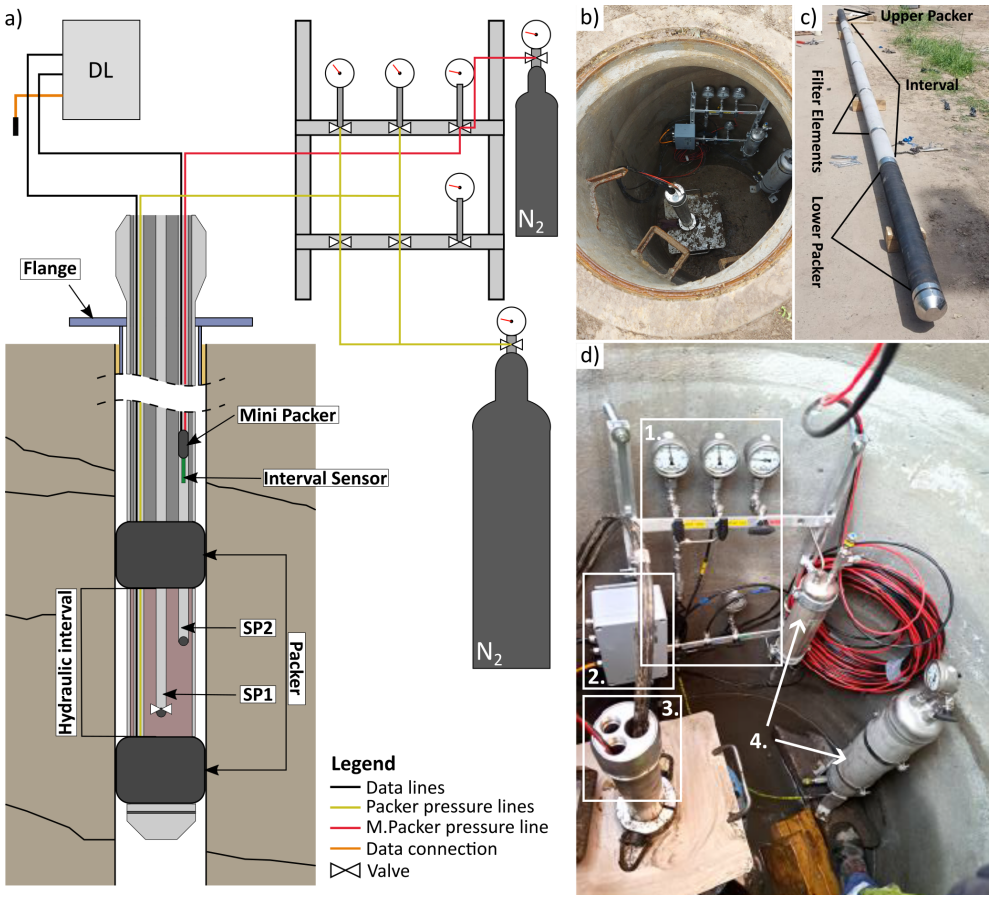

Figure 6. **(a)** Schematic illustration of the Standpipe Double Packer System (SPDP) as installed within six boreholes of the project, **(b)** data cavern with SPDP installations, **(c)** SPDP interval section with filter elements and packers **(d)** detail view on data cavern installations showing flowboard with (1) manometers and valves for packer-pressure regulation, (2) data logger, (3) SPDP with openings of SP1, SP2 and operation line for packer regulation, and (4) Nitrogen tanks for the regulation of packer pressures.

the in-situ water. Equilibration of pressure conditions, until steady-state conditions were reached followed the installation and inflation of the SPDP system.

3.4 Sampling and sample handling

Claystone drill core samples are prone to alteration processes after being retrieved from their in-situ conditions, potentially introducing irreversible changes in their properties (Ma and Zoback, 2018). Unloading due to the loss of the formation's confining pressure can lead to decompaction and result in fracturing, such as the initiation of micro-fractures (Basu et al., 2020). The exposure to air leads to the loss of pore water, hence desaturation, a reduced saturation ratio, shrinkage, and potential mineral precipitation, causing desiccation damage. In contrast, contact with brine can result in water uptake, dissolution, and swelling (Ewy, 2015). These alterations imply changes in the porosity, permeability, and mechanical characteristics of claystone drill core samples during and after retrieval. Consequently, appropriate drill core and sample handling is required to minimize alteration processes of the sample material and consequent changes in petrophysical and mechanical properties of the claystones.

A protein-based polymer drilling additive (Pure-Bore©) was used to prevent mixing of drilling fluid and formation water and associated disequilibria that can lead to clay mineral swelling. Drill cores with a diameter of 101 mm were cored in 3 m PVC liner intervals, which were cut into 1 m-long segments. Samples of approx. 1 cm thickness were cut from the individual core end-faces right after core extraction for geochemical testing. The core segments were closed with PVC end caps. Every second core segment was individually sealed in opaque aluminum foil, and de-aired to maintain a constant water content. For transport and storage, the cores were stored in wooden boxes. The tightness of the sealing was controlled regularly, and renewed if necessary.

3.5 Laboratory investigations

A comprehensive, multidisciplinary laboratory program is currently being conducted on core material from the boreholes. This program encompasses methods for geochemical characterization of the Amaltheenton-Fm, petrophysical investigations, as well as mechanical laboratory tests. In this contribution, the presentation and analysis of data focuses on selected methods, aiming for a first characterization of the Amaltheenton-Fm. Results of other lithologies and formations are concisely presented. A comprehensive analysis of the full set of laboratory and borehole data is outside the scope of this contribution and will be addressed in individual parameter studies.

Core samples from boreholes BO1.0–BO5.0 were continuously sampled at intervals ranging from 0.5 to 1 m for geochemical analysis. Rock-Eval pyrolysis was employed using a Rock-Eval 7 device by Vicini Technologies to determine already generated, free hydrocarbon S1 ($\mathrm{mg\,HC\,(g\ rock)^{-1}}$), the hydrocarbon potential S2 ($\mathrm{mg\,HC\,(g\ rock)^{-1}}$), and generated CO_2 S3 ($\mathrm{mg\,CO_2\,(g\ rock)^{-1}}$). Total Organic Carbon (TOC), normalized Hydrogen Index (HI), and Oxygen Index (OI) were calculated. Additionally, the organic (TOC) and inorganic carbon content (TIC, and related carbonate content) were derived based on the pyrolysis data. The temperature of maximum hydrocarbon generation ($T_{\max}$) was determined and corrected to Rock-Eval standards. For a detailed methodology of the applied measurements see Burnaz et al. (2024) and references therein.

Quantitative X-ray diffraction (XRD) analysis was conducted on powdered bulk materials to obtain the mineralogical composition of the target formation. Gently crushed bulk materials were spiked with $0.2\,\mathrm{g\,g^{-1}}$ internal standard (α-Al_2O_3) for accuracy control and ground in a McCrone Micronizing mill, adding ethanol as cooling lubricant to prevent heat- and mechanical strain damage. The air-dried powders were measured on a Bruker D8 diffractometer using Cu Kα radiation (40 kV, 40 mA). The mineralogical composition was quantified based on Rietveld refinement employing the BGMN-based software Profex in combination with customised clay-structure models (Ufer et al., 2008; Doebelin and Kleeberg, 2015; Ufer and Kleeberg, 2015). The major elemental composition was obtained from X-Ray fluorescence. Powder pellets prepared from 8 g of powdered bulk material ($< 63\,\mu\mathrm{m}$) combined with 2 g of Fluxana CEREOX wax and pressed for 120 s at 19.2 MPa. The analysis was performed on an energy dispersive polarised SPECTRO XEPOS ED(P)-X-Ray fluorescence instrument (limit of detection $\leq 1.4\,\mu\mathrm{g\,kg^{-1}}$) (Grohmann et al., 2023). Every sample was measured twice, rotating the pellet in between. Subsequently, mean values were calculated for the two measurements. In this contribution, the presentation of the elemental analysis results focuses on aluminum, silicon, and iron.

Porosities were calculated on several specimens from intact core sections of the boreholes BO1.0–BO5.0. Bulk densities and skeletal densities for porosity determination were derived from caliper and weight measurements, and He-pycnometry, respectively, following the methods described by Gaus et al. (2022) and references therein.

Permeability was measured under unconfined conditions using a modified pycnometry-based method. The applied modifications build upon concepts and experimental techniques reported by Li et al. (2006), Gaus et al. (2019), and Khajooie et al. (2025). In this approach, permeability is measured via radial gas uptake by sealing the axial surfaces of the core sections using epoxy. The measurements were then evaluated based on mathematical solutions for diffusion in a cylinder in the radial direction, along with a diffusivity equation that relates diffusion to permeability and porosity (Crank, 1975; Li et al., 2006; Khajooie et al., 2025). Nitrogen was used as the permeating gas.

4 Results

4.1 Lithological borehole sequences

Lithological borehole interpretations were derived from the geophysical logging data and from geochemical analysis of the extracted core material. Lithological borehole profiles of selected boreholes are presented in Fig. 7 alongside the respective spectral (SGR) and computed GR (CGR) signals.

At location BO1, the first 14 m of the boreholes penetrated Quaternary unconsolidated sediments. Between 14 and 15 m depth, a peak in GR-readings indicates a layer of Cretaceous glauconitic sandstones, which can be identified as part of the Lower Cretaceous Hils-Formation. From 15 m depth onwards, grayish claystones (Opalinuston-Fm/Jurensismergel-Fm) extend to a depth of approximately 46 m. At this point, a peak in the GR-signal (168 API) indicates the transition into the Posidonienschiefer-Fm. The Amaltheenton-Fm follows from a depth of 65 m and constitutes the borehole lithology down to the final depth of 98 m. The boreholes at locations Mainzholzen and Hunzen penetrated a succession of Quaternary sediments followed by the Opalinuston-Fm/Jurensismergel-Fm, and the Posidonienschiefer-Fm, overlying the Amaltheenton-Fm. In BO4.0, both the Opalinuston-Fm/Jurensismergel-Fm and Posidonienschiefer-Fm are entirely absent. Below approximately 6 m of unconsolidated Quaternary/Tertiary sediments, the Amaltheenton-Fm was encountered and constitutes the entire borehole lithology to the final depth of 95 m. The boreholes at the Bensen location (BO5.0 and BO5.1) penetrated the Posidonienschiefer-Fm below a few metres of Quaternary/Tertiary overburden, while the Opalinuston-Fm/Jurensismergel-Fm is absent. The Amaltheenton-Fm was encountered at a depth of 37 m (BO5.0) and 38 m (BO5.1), respectively.

Where existent, the Posidonienschiefer-Fm stands out in GR logging signals as a distinct peak with high GR readings

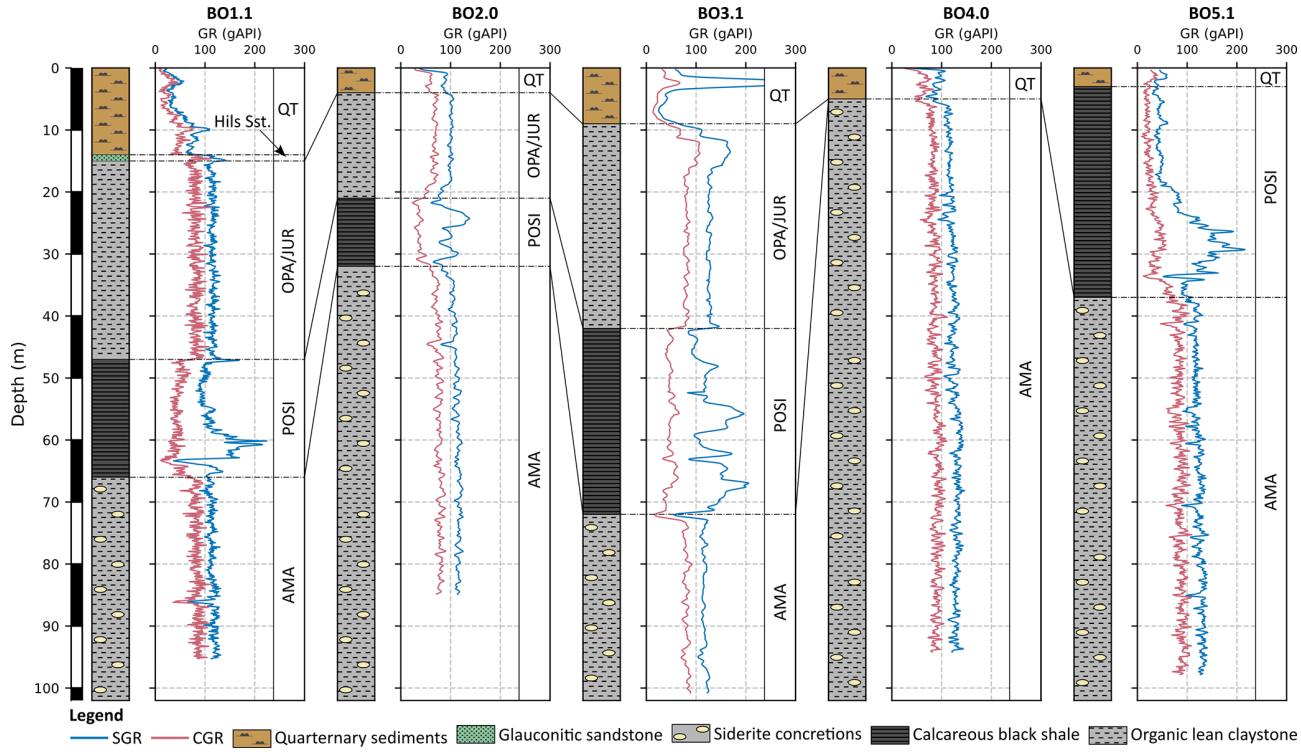

Figure 7. Lithostratigraphic correlations of selected boreholes from each Maturity-project drilling location with gamma-ray logging signals (SGR = Spectral Gamma-Ray; CGR = Computed Gamma-Ray). Qt. = Quaternary, Sst = Sandstone, JUR = Jurensismergel-Fm, OPA = Opalinuston-Fm, POSI = Posidonienschiefer-Fm, AMA = Amaltheenton-Fm.

(> 140 API) due to its high organic-matter content (mean TOC from 6.4 wt. % to 9.7 wt. %) and a correspondingly high uranium concentration. The Posidonienschiefer-Fm serves as a marker horizon for the stratigraphic classification of the boreholes. Its pronounced geophysical and geochemical signatures make it a valuable tool for the regional correlation and stratigraphic interpretation between the individual borehole locations. The transition to the Amaltheenton-Fm is indicated by a decrease in the gamma-ray log response. The Amaltheenton-Fm is characterized by constant GR readings between 110–120 API. Here, little variation in the logging signal indicates a similar composition between the individual locations. In the extracted drill cores, the Amaltheenton-Fm generally appears as a gray, fine bedded claystone with a frequent appearance of yellow-brownish carbonate concretions (Fig. 8) identified as siderite concretions. The occurrence of siderite concretions varies from millimetre- to centimetre-long spheroidal nodules to decimetre-thick sideritic "lumps".

4.2 Geochemical and mineralogical characteristics

Spectrometric ratios of the elements Th, K, and U were derived from the SGR logging signals. Little variation and consistent clustering of Th/K ratios (Fig. 9a) can be observed in the Amaltheenton-Fm between the individual test sites, suggesting a similar clay mineral assemblage throughout the formation. The Th/K cross plot suggests a clay mineralogy dominated by mixed-layer clay with mean Th/K ratios between 7.1 (BO1.1) and 7.98 (BO3.0). Mean Th/U ratios range between 4.87 (BO2.0) and 7.04 (BO3.0). In BO1.1, Th/U ratios of 6.82 are almost equally high as those in BO3.0, whereas BO4.0 and BO5.0 show values closer to BO2.0, at 5.84 and 4.94, respectively. However, generally, the Th/U ratios show overlapping clustering as indicated in Fig. 9b.

Quantitative XRD and XRF analyses were conducted to determine the mineralogical and geochemical composition of the Amaltheenton-Fm. The results characterize the Amaltheenton-Fm as a claystone dominated by high clay contents ranging between 58 wt % (BO1.0) and 75 wt % (BO2.0) (Fig. 10). The framework silicates Quartz and Feldspars contribute between 15 wt. % to 23 wt. %, and 7 wt. % to 12 wt. %, respectively. The carbonate content within the Amaltheenton-Fm is generally low with a maximum concentration of 8 wt. % in borehole BO5.0. Exceptionally high but spatially confined carbonate contents of up to 80 wt. % were observed for several carbonate concretions, i.e., siderite, across all locations in the Amaltheenton-Fm. Quantitative XRD analyses revealed siderite as primary component of these samples, endorsed by increased Fe values from XRF analysis (Fig. 10b). Siderite concretions occur in the Amaltheenton-Fm in all boreholes but were not sampled

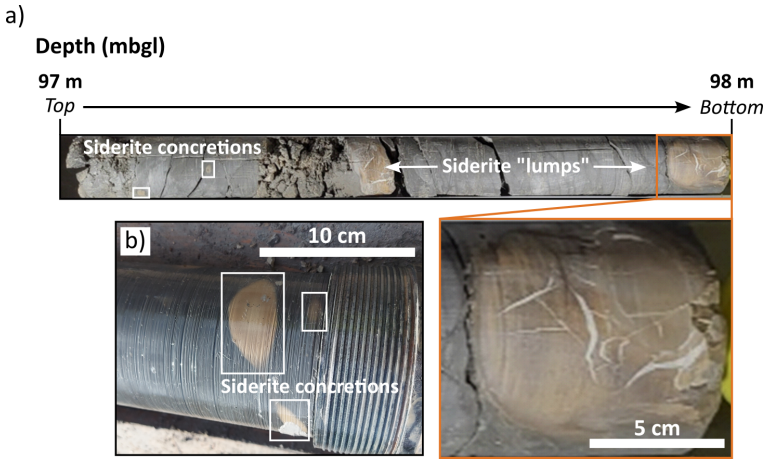

Figure 8. Exemplary rock core sections of the Amaltheenton-Fm with emphasis on siderite concretions of variable size and shape: **(a)** Drill core section from borehole BO2.0 between 97 and 98 m below ground level (mbgl), and **(b)** core section from borehole BO4.0 with indication of siderite nodules.

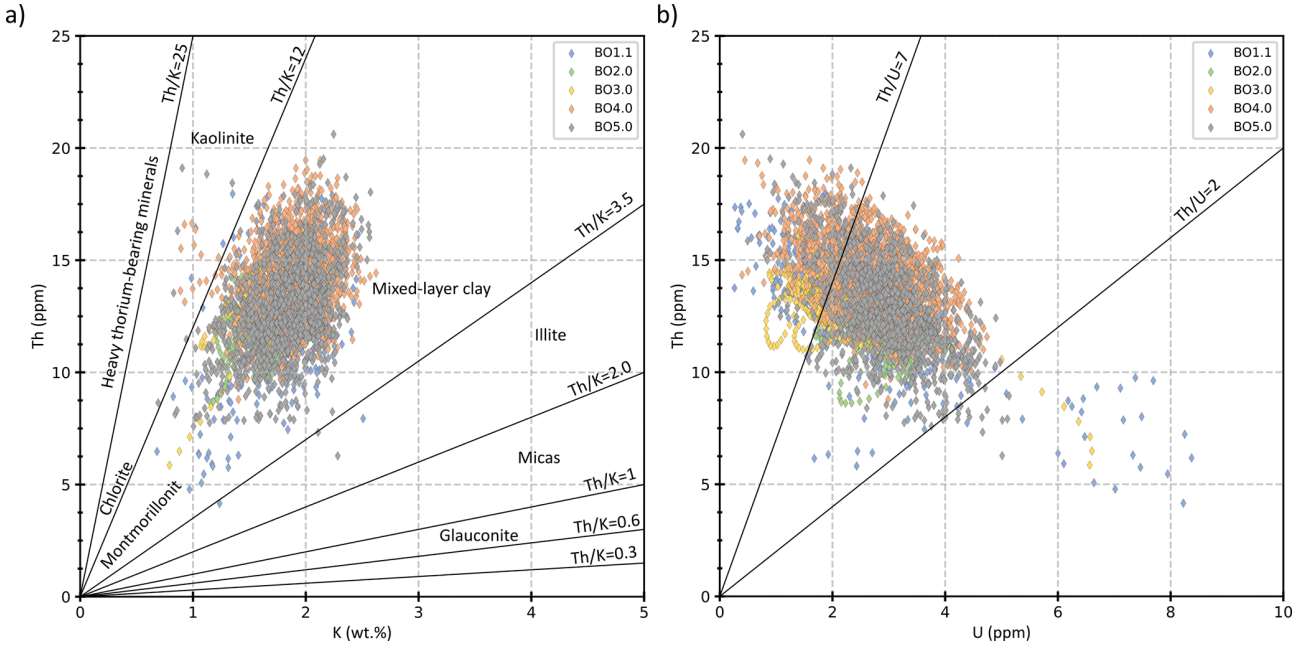

Figure 9. Elemental ratios of the Amaltheenton-Fm from SGR logging signals: **(a)** Thorium versus potassium mineral identification plot from Schlumberger (2009) with plotted SGR readings from the boreholes BO1.1, BO2.0, BO3.0, BO4.0, BO5.0; **(b)** Thorium versus uranium plot.

to the same extent, resulting in an apparent siderite abundance in boreholes BO2.0 and BO4.0 in Fig. 10. According to the classification scheme provided by Lazar et al. (2015), the Amaltheenton-Fm can be defined as argillaceous fine-grained sedimentary rock. Table 2 provides a summary of the general mineralogical composition of the Amaltheenton-Fm. The results align with findings from Gaus et al. (2022) on sample material from the old core material.

4.3 Thermal maturation sequence

The vitrinite reflectance was determined on selected samples obtained from core sections from five of the boreholes (BO1.0 - BO5.0). Most of these samples are extracted from the Amaltheenton-Fm borehole intervals, since the Posidonienschiefer-Fm is depleted in vitrinite (Littke et al., 1988). Vitrinite reflectance in boreholes BO1.0 and BO2.0 is similar at about 0.52 % and 0.48 % VRr, respectively, while higher values are recorded for boreholes BO3.0, BO4.0, and BO5.0, i.e.,0.70 %, 0.87 %, 1.51 % VRr, respectively). These

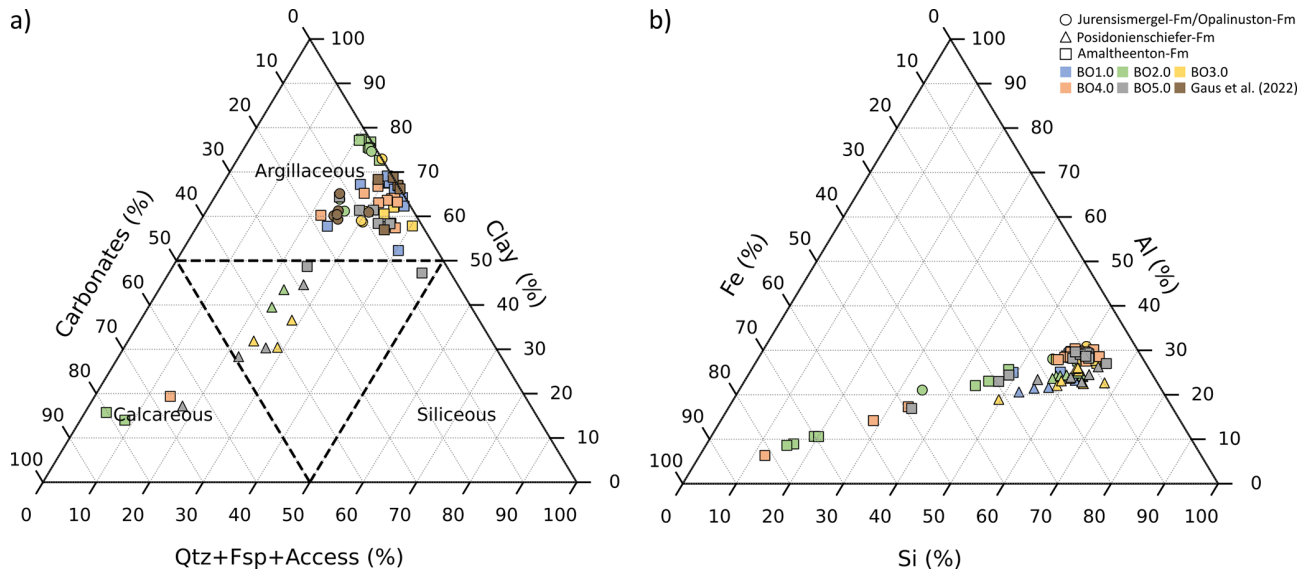

Figure 10. Ternary plots of **(a)** mineralogical composition from XRD analysis with data from the Maturity-project boreholes and old boreholes after Gaus et al. (2022). Nomenclature guidelines for the composition of fine-grained sedimentary rocks are added based on Lazar et al. (2015); **(b)** the Fe-Si-Al phase from XRF analysis of boreholes BO1.0, BO2.0, BO3.0, BO4.0, and BO5.0.

Table 2. Summary of mean XRD-derived mineralogical composition of the Amaltheenton-Fm. Standard deviations are given beside the mean values. Sample populations are indicated for each borehole with (#).

Borehole	Quartz (wt. %)	Clays (wt. %)	Carbonates (wt. %)	Feldspars (wt. %)	Accessories (wt. %)
BO1.0 (#9)	19.94 ± 3.34	64.63 ± 4.76	2.47 ± 2.49	8.62 ± 0.46	4.34 ± 1.04
BO2.0 (#6)	14.58 ± 1.80	75.69 ± 1.67	1.17 ± 0.65	7.41 ± 0.26	1.14 ± 0.47
BO3.0 (#4)	17.15 ± 2.20	59.86 ± 1.76	4.82 ± 2.55	11.81 ± 1.38	4.11 ± 1.87
BO4.0 (#8)	19.35 ± 3.48	63.11 ± 2.67	5.59 ± 4.96	8.75 ± 2.83	3.28 ± 0.59
BO5.0 (#6)	22.84 ± 6.66	58.40 ± 5.46	8.00 ± 2.42	6.96 ± 0.96	3.80 ± 0.60

values agree well with those published earlier for adjacent boreholes on the southwestern flank of the Hils Syncline and with values from numerous Jurassic outcrop samples (Castro-Vera et al., 2024; Littke et al., 1988).

Further information on thermal maturity is provided by elemental analysis and Rock-Eval data. Average Rock-Eval data for the drilled formations is summarized in Table 3. TOC and carbonate contents are high in the Posidonienschiefer-Fm, moderate in the Jurensismergel-Fm/Opalinu Clay Fm, and low in the Amaltheenton-Fm. In Fig. 11, Rock-Eval derived data from BO2.0 is plotted against depth to exemplarily visualize this trend.

Carbonate content is not significantly affected by thermal maturity as visible from a comparison of boreholes BO1.0 and BO5.0, while TOC values decrease from the immature to the overmature state, e.g., in the Posidonienschiefer-Fm from about 10 % to about 6 %. This observation is in accordance with the mass balance results published in Rullkötter et al. (1988). Furthermore, HI values are very high in the Posidonienschiefer-Fm, moderate in the Jurensismergel-Fm/Opalinuston-Fm, and rather low in the Amaltheenton-Fm. However, during thermal maturation, the HI is much reduced due to petroleum generation and expulsion; therefore, values in the Posidonienschiefer-Fm are much lower in BO5.0 (Table 3). This trend is also observed for the Amaltheenton-Fm, but it is less obvious, because initial values in, e.g., borehole BO1.0 are already low.

Concerning these thermal maturity comparisons, it must be emphasized that the same formation should always be compared. This is done here, but not always the same stratigraphic range has been drilled. An almost complete profile of Posidonienschiefer-Fm only exists for BO3.0 and BO5.0, and the Amaltheenton-Fm was drilled in thicknesses ranging from less than 30 m to almost 100 m.

Aside from HI values, Rock-Eval T_{max} values are dependent on thermal maturity. In the Posidonienschiefer-Fm, T_{max} values increase from BO1.0/BO2.0 (about 420 °C) to BO3.0 (about 441 °C) and BO5.0 (463 °C). A common plot on thermal maturity is the HI (Hydrogen Index) versus T_{max} diagram (Fig. 12). Standard lines separating between

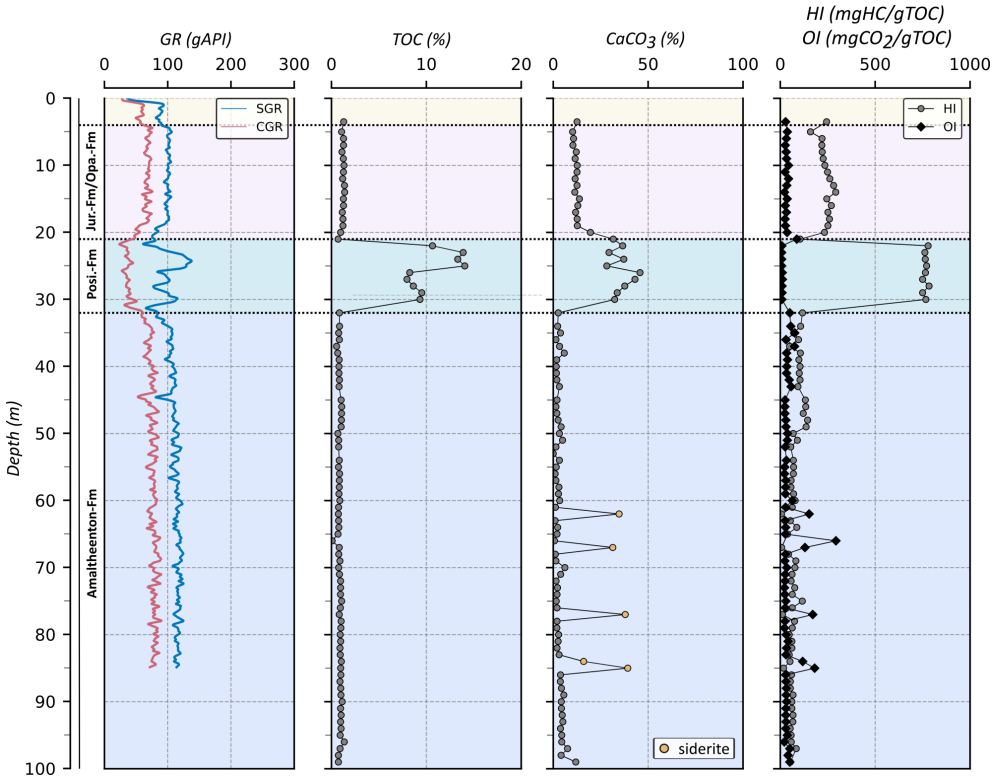

Figure 11. Bulk geochemical data of BO2.0. Total organic carbon (TOC), $CaCO_3$, and hydrogen index (HI) data were derived from Rock-Eval pyrolysis. In addition, spectral- and computed gamma-ray (SGR and CGR, respectively) are given.

Table 3. Summary of organic and inorganic carbon content (TOC, TIC), calcite content ($CaCO_3$), hydrogen index (HI), oxygen index (OI), peak S2 temperature (T_{max}), and vitrinite reflectance for the Amaltheenton-Fm from boreholes BO1.0 to BO5.0. Sample populations are indicated for each borehole with (#).

Borehole	Formation	TOC ± Std. (wt. %)	TIC ± Std. (wt. %)	$CaCO_3$ (wt. %)	HI ± Std. (mg HC (g TOC)$^{-1}$)	OI ± Std. (mg CO_2 (g TOC)$^{-1}$)	Tmax ± Std. (°C)	VRr ± Std. (VRr %)
BO1.0	JM/OPA (#29)	2.10 ± 0.33	0.85 ± 0.58	7.06	225 ± 39	21 ± 7	434 ± 3	
	POSI (#17)	9.73 ± 3.90	4.42 ± 2.92	36.69	6845 ± 49	7 ± 1	418 ± 5	
	AMA (#27)	0.84 ± 0.10	0.20 ± 0.13	1.66	128 ± 38	39 ± 15	437 ± 4	0.52 ± 0.04 (#5)
BO2.0	JM/OPA (#17)	1.23 ± 0.11	1.50 ± 0.25	12.45	242 ± 30	32 ± 6	430 ± 3	
	POSI (#10)	9.63 ± 3.91	4.28 ± 0.68	35.52	700 ± 210	16 ± 25	422 ± 1	
	AMA (#59)	0.88 ± 0.14	0.37 ± 0.22	3.07	76 ± 27	34 ± 12	431 ± 3	0.48 ± 0.04 (#5)
BO3.0	JM/OPA (#24)	1.71 ± 0.40	0.84 ± 0.29	6.97	294 ± 103	24 ± 25	435 ± 4	
	POSI (#9)	8.56 ± 1.01	5.80 ± 0.54	48.14	652 ± 28	4 ± 1	441 ± 2	
	AMA (#10)	0.74 ± 0.07	0.37 ± 0.14	3.07	151 ± 31	38 ± 12	444 ± 3	0.70 ± 0.05 (#5)
BO4.0	AMA (#65)	0.83 ± 0.11	0.43 ± 0.51	3.57	78 ± 22	40 ± 22	447 ± 2	0.87 ± 0.08 (#5)
BO5.0	POSI (#21)	6.40 ± 1.15	4.80 ± 140	39.84	60 ± 6	4 ± 1	463 ± 5	
	AMA (#52)	0.81 ± 0.16	0.38 ± 0.22	3.15	25 ± 13	65 ± 61	462 ± 28	1.51 ± 0.08 (#10)

immature, mature, and overmature conditions for petroleum generation (0.5 VRr %, and 1.2 VRr %, respectively) are additionally plotted. However, these lines should be considered as a rough orientation. The progress in thermal maturity is obvious from the plotted data. For BO4.0, only Amaltheenton-Fm data is available; however, BO4.0 is adjacent to the old Harderode borehole (Har), which penetrated the Posidonienschiefer-Fm. The respective data published by Rullkötter et al. (1988) fits also well into this trend. For BO5.0, only Posidonienschiefer-Fm samples can be used, because pyrolysis peaks for the Amaltheenton-Fm are too small to evaluate T_{max} values (see also very low HI values; Table 3).

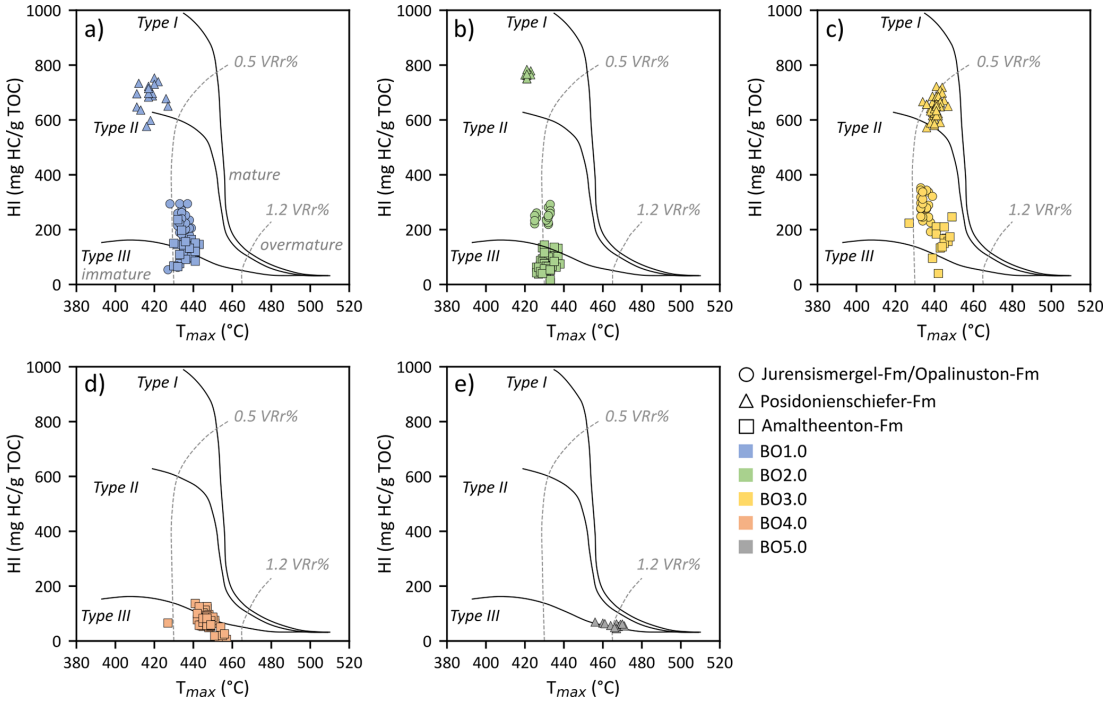

Figure 12. Hydrogen Index vs. Tmax crossplots outlining the kerogen types I, II, and III and the thermal maturity for samples of Jurensismergel-Fm (JM)/Opalinuston-Fm (OC), Posidonienschiefer-Fm (Posi), and the Amaltheenton-Fm (AMA) from the boreholes drilled in the MATURITY project: **(a)** BO1.0 (blue), **(b)** BO2.0 (green), **(c)** BO3.0 (yellow), **(d)** BO4.0 (orange), and **(e)** BO5.0 (grey).

Table 4. Basic petrophysical rock data of the Amaltheenton-Fm derived from logging and laboratory data. Log densities and porosities were derived from gamma-density logs. Laboratory data was determined via He-pycnometry and caliper measurements.

Borehole	Mean V_p ($m\,s^{-1}$)	Gamma-Density ($g\,cm^{-3}$)	Gamma-Porosity (%)	Bulk Density ($g\,cm^{-3}$)	Porosity (%)	Permeability ($\times 10^{-19}\,m^2$)	Equivalent hydraulic conductivity ($\times 10^{-12}\,m\,s^{-1}$)
BO1.0	–	–	–	2.31	12.47	1.47	1.81
BO1.1	2367	2.45	14.57	–	–	–	–
BO2.0	2301	–	–	2.35	13.7	1.48	1.81
BO3.0	2702	2.51	11.26	2.45	9.15	0.89	1.09
BO3.1	2681	–	–	–	–	–	–
BO4.0	3050	–	–	2.48	8.96	0.13	0.15
BO5.0	2555	–	–	2.46	10.26	0.16	0.20
BO5.1	2538	2.50	11.56	–	–	–	–

4.4 Petrophysical and hydrogeological characteristics

Different geophysical logging methods were applied to assess the in-situ petrophysical properties. Mean compressional wave velocities (V_p) from the Amaltheenton-Fm show an increasing trend from BO1.1/BO2.0 (2367 and 2302 $m\,s^{-1}$) to BO4.0 (3050 $m\,s^{-1}$), while a decrease is observed between BO4.0 and both boreholes at the borehole location Bensen (BO5.0 and BO5.1 with 2555 and 2538 $m\,s^{-1}$, respectively see Fig. 13a). Gamma-density logs (GGD) from BO1.1, BO3.0, and BO5.1 are additionally presented in Fig. 13. Mean densities from the logging data of the Amaltheenton-Fm sections within those three boreholes are 2.45, 2.51, and 2.50 $g\,cm^{-3}$. Mean porosities were derived at 14.57 %, 11.26 %, and 11.56 %, respectively. In laboratory measurements, mean bulk densities range between 2.31 $g\,cm^{-3}$ (BO1.0) and 2.49 $g\,cm^{-3}$ (BO4.0), while porosities derived from He-pycnometry are between 8.96 % and 13.58 % in BO4.0 and BO2.0, respectively. A similar trend to V_p velocities is observed in the lab density data, showing an increase in density between the borehole locations BO1.0 and BO4.0, whereas densities in BO5.0 average slightly below those from BO4.0 with 2.46 $g\,cm^{-3}$. Conversely, porosities initially decrease

in the order BO2.0 > BO1.0 > BO3.0 > BO4.0, but show an increase between BO4.0 (8.96 %) and BO5.0 (10.26 %). Permeability data from unconfined conditions further reflects variations seen in porosities. Between BO2.0 and BO4.0, the permeability decreases from 1.48×10^{-19} to $1.25 \times 10^{-20}\,m^2$, then the permeability slightly increases to $1.61 \times 10^{-20}\,m^2$. However, no significant differences were observed between BO1.0 and B02.0. Table 4 summarizes log- and lab-derived petrophysical data from the Amaltheenton-Fm.

A first series of hydraulic tests from boreholes BO1.0, BO2.0, BO3.1, and BO4.0 was conducted and evaluated. The results are presented in Table 5. Hydraulic conductivities span two orders of magnitude, ranging from $1.15 \times 10^{-7}\,m\,s^{-1}$ (BO4.0) to $2.68 \times 10^{-5}\,m\,s^{-1}$ (BO1.0).

5 Discussion

The following subchapters discuss the results of the present study with emphasis on the prerequisites and objectives defined in Sects. 1.1 and 1.2, thereby placing the findings into the broader context of the MATURITY project and providing a framework for subsequent, more detailed investigations.

5.1 Depositional environment and mineralogical composition of the Amaltheenton-Fm

XRD and XRF analyses conducted on Amaltheenton-Fm samples from all boreholes clearly indicate clay minerals as being the dominant mineral type (58 wt %–75 wt %) and defining the Amaltheenton-Fm as argillaceous claystone. Th/K ratios derived from gamma-ray logs suggest a mixed-layered clay mineralogy that exhibits tight overlap between the individual borehole locations. Carbon data (TOC, TIC) also demonstrate low variance within the Amaltheenton-Fm. However, the mean Th/U ratios of the Amaltheenton-Fm show some slight variability, ranging between a factor of approximately 5 in boreholes BO2.0, BO4.0, and BO5.0, and a factor of approximately 7 in boreholes BO1.1 and BO3.0, which might be attributed to various reasons. Th/U ratios between 2 and 7 are associated with a marine depositional environment and moderate terrigenous supply, while values > 7 indicate continental, oxidizing conditions, and values < 2 marine, reducing conditions (Adams and Weaver, 1958; Rider, 2000; Klaja and Dudek, 2016; Bataller et al., 2022). A detailed paleo-environmental study on samples from boreholes BO2.0 and the adjacent borehole Wickensen WIC) by Burnaz et al. (2024) revealed a shallow marine depositional setting with effective circulation under predominantly oxic bottom water conditions and terrigenous clastic input for the Amaltheenton-Fm. Similar findings were recently published by Wijesinghe et al. (2025) on samples from the Hunzen borehole. Generally, this corresponds to the detected Th/U ratios. However, higher Th/U ratios, close to 7, as seen in BO1.1 and BO3.0, might be due to different stratigraphic ranges within the Amaltheenton-Fm and slightly divergent environmental conditions during deposition, characterized by stronger continental influence. Differences in Th/U ratios are also likely to be a result of secondary uranium mobilization and fluid migration from the overlying Posidonienschiefer-Fm, resulting in lower values at locations BO2.0, BO4.0, and BO5.0.

5.2 Thermal maturity and maximum burial evolution of the Amaltheenton-Fm

The increase in thermal maturity is documented by several parameters (VRr, TOC, HI, T_{max}). The maturity trend that was established for the Hils Syncline follows published data (see Littke et al., 1988; Castro-Vera et al., 2024), where SE-NW directed thermal maturity increase is interpreted as related to deep burial. Measured vitrinite reflectance values can be converted into maximum burial temperatures based on an empirical equation published by Barker and Pawlewicz (1994):

$$T_{peak}(\text{burial}) = (\ln(\text{VRr}) + 1.68)/0.0124 \quad (2)$$

When applied to BO1.0, BO2.0, BO3.0, BO4.0, and BO5.0 (with VRr % values of approximately 0.52, 0.48, 0.70, 0.87, and 1.51, respectively), the resulting maximum burial temperatures are 83, 76, 107, 124, and 169 °C. Maximum burial depths can be established from T_{peak}, incorporating the sediment water interface temperature (SWIT) and the geothermal gradient at the time of maximum burial. Based on the 3D model provided by Castro-Vera et al. (2024), the SWIT temperature during deepest burial (latest Early Cretaceous) is sampled at approx. 24 °C (personal communication with Leidy Castro-Vera) while a geothermal gradient of 30 °C was assumed. Maximum burial temperatures and depths for the Amaltheemton-Fm from all investigated locations are given in Table 6. Note that T_{peak} values established via Eq. (2) and related burial depths reached over geologic times are not directly related to T_{max} values obtained from Rock-Eval pyrolysis measurements. According to the temperatures calculated via Eq. (2), BO1.0 and BO2.0 are immature, BO3.0 and BO4.0 have reached the oil generation stage (oil window), and BO5.0 is in the gas generation stage. This fits well with the results from Rock-Eval pyrolysis. It should be noted that this temperature and burial depth calculation via Eq. (2) does not consider the exact burial and temperature history, but it is a simple yet useful approximation. Short periods at the maximum temperature, e.g., during igneous intrusions, would lead to higher temperatures. One important aspect is attributed to the subtle difference between boreholes BO1.0 and BO2.0. The initial expectation was that BO1.0 situated outside of the Hils Syncline close to the southern tip of Sack Syncline, might be thermally less mature than BO2.0. This is not the case according to the collected data; thermal maturity is very similar, and T_{max} values

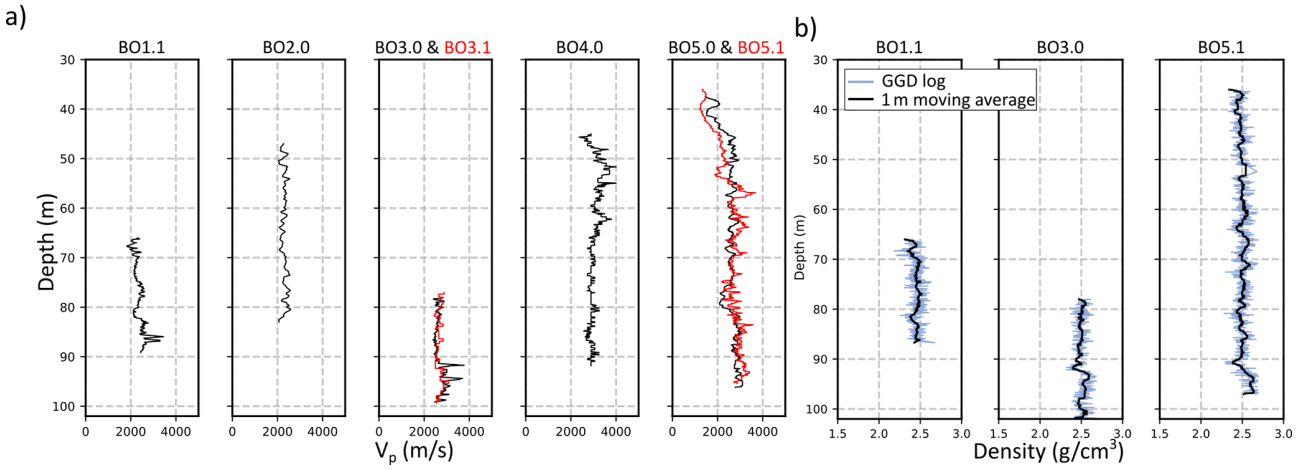

Figure 13. Logging sections in the Amaltheenton-Fm: **(a)** Compressional wave velocities (V_p) from sonic logs, and **(b)** gamma-density logs (GGD) of the boreholes BO1.1, BO3.0, and BO5.1.

Table 5. Summary of hydraulic test results. Presented data was evaluated from pulse withdrawal (PW) and slug withdrawal tests (SW). T = transmissivity, K = hydraulic conductivity, n = flow dimension.

Borehole	Test Type	Investigation Depth (m)	Interval Length (m)	Static Pressure (kPa)	Minimum Pressure (kPa)	T ($m^2\,s^{-1}$)	K ($m\,s^{-1}$)	n
BO1.0	SW	78.50–82.84	4.34	609.0	342.0	3.12×10^{-5}	2.68×10^{-5}	1.4
BO2.0	SW	63.0–70.50	7.50	631.19	543.61	1.91×10^{-5}	1.62×10^{-6}	1.7
BO3.1	PW	92.0–96.34	4.34	454.52	10.76	3.02×10^{-5}	6.95×10^{-6}	2.9
BO4.0	SW	31.90–39.00	7.10	339.65	225.0	8.17×10^{-7}	1.15×10^{-7}	2.3

even tend to be slightly higher at BO1.0 than at BO2.0. Such subtle differences in the thermal maturity of immature rocks can well be investigated by biomarker studies in the future.

5.3 The influence of thermal maturity and maximum burial on physical rock properties

The thermal maturity range of the Amaltheenton-Fm measured at locations BO1 (0.50 VRr %), BO2 (0.48 VRr %), BO3 (0.70 VRr %), BO4 (0.85 VRr %), and BO5 (1.51 VRr %) is similar to that observed in nearby sections drilled by the old 1980's boreholes (Littke et al., 1988; Gaus et al., 2022). In their study, Gaus et al. (2022) also published an initial dataset on the petrophysical properties of the Amaltheenton-Fm, based on samples from the boreholes Wenzen, Dielmissen, Dohnsen, Harderode, and Haddessen. Porosities determined by He-pycnometry initially follow a decreasing trend with increasing thermal maturity, ranging from 14.69 % at 0.48 VRr % (Wenzen) to 7.67 % at 0.73 VRr % (Dohnsen), while bulk densities range between 2.32 g cm^{-3} (Wenzen) and 2.56 g cm^{-3} (Harderode). Despite strong uplift, the data presented by Gaus et al. (2022) is indicative of gradual compaction trends due to variable maximum burial depths. However, a slight increase in porosity is observed, reaching 8.27 % in the Haddessen borehole, with thermal maturity continuously rising to 1.45 VRr % while the bulk density is slightly decreasing to 2.48 g cm^{-3}. Castro-Vera et al. (2024) attributed the trend towards increased porosities at the highest maturity to gas overpressures generated within the Posidonienschiefer-Fm, and resulting overpressure transfer to the surrounding formations. In addition to gas generation, overpressure may also have developed due to undercompaction caused by rapid burial and associated fluid retention, leading to the buildup of excess pore pressure (Castro-Vera et al., 2024).

A similar trend is observed in data from the MATURITY project boreholes from both logging and lab data. Densities and porosities derived from the GGD logging signals for the boreholes BO1.1, BO3.0, and BO5.1 are presented together with respective lab data from the core material of all borehole locations in Fig. 14b–d. Regarding the thermal maturity, the Amaltheenton-Fm from those boreholes is similar to Wenzen (similar to BO1.0 and BO2.0), Dohnsen, Harderode, and Haddessen, respectively. Compressional wave velocities (V_p) usually increase with burial depth due to compaction and cementation processes and reduced elasticity. Our mean V_p values show a progressive increase in the order BO2.0 < BO1.1 < BO3.0 < BO5.0 < BO4.0. V_p values from those boreholes are plotted versus their respective thermal maturity quantified by vitrinite reflectance. A very good

Table 6. Estimated maximum burial temperatures (T_{peak} (burial)) and depths from vitrinite reflectance for the boreholes BO1.0–BO5.0. 3D modelled maximum burial depth adapted from Castro-Vera et al. (2024) and modelled T_{peak} values based on personal communication with Leidy Castro-Vera.

Borehole	Vitrinite reflectance (VRr %)	T_{peak} (burial) (°C)	Maximum burial depth (m)	Tpeak burial 3D model (°C)	Maximum burial depth 3D model (m)
BO1.0	0.52	83	1970	93	1550
BO2.0	0.48	76	1730	83	1400
BO3.0	0.70	107	2770	116	2100
BO4.0	0.87	124	3330	127	2440
BO5.0	1.51	169	4830	163	3300

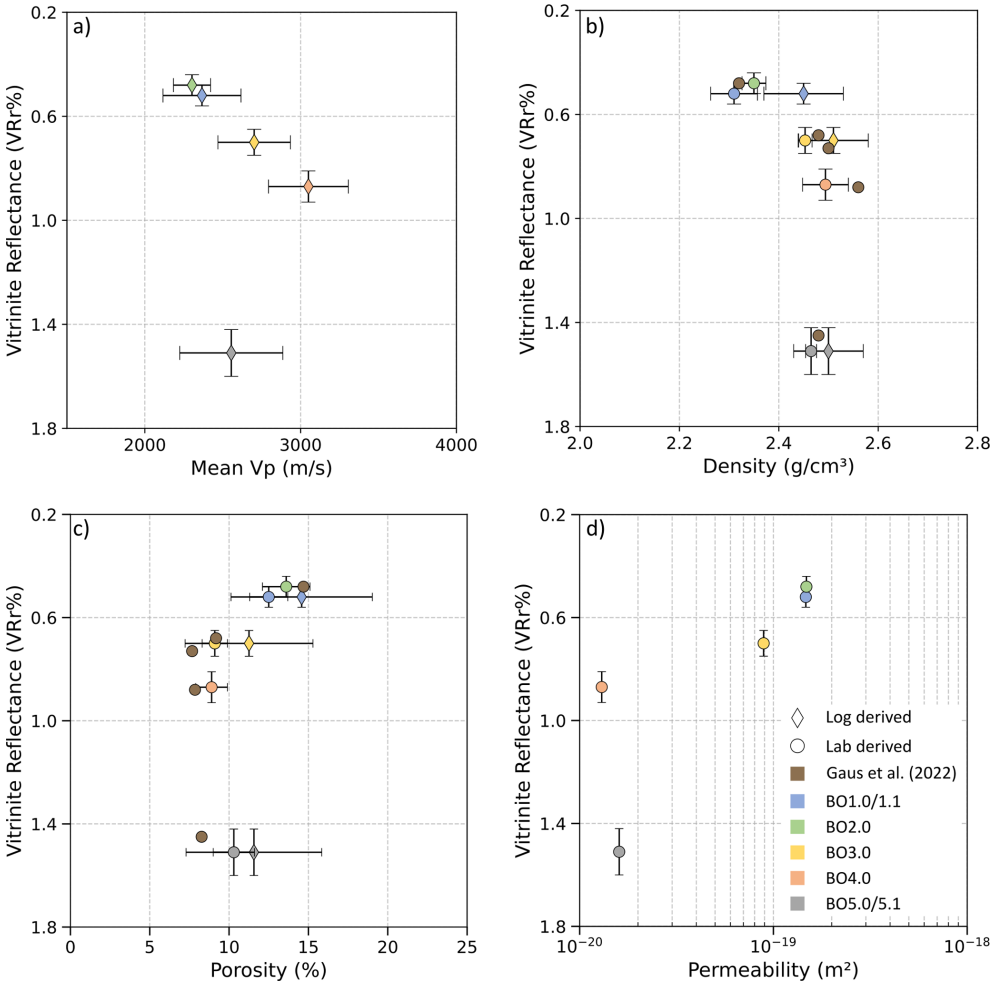

Figure 14. Vitrinite reflectance plotted against selected properties of the Amaltheenton-Fm from logging (rhombus) and lab (circle) data complemented by data from old boreholes after Gaus et al. (2022): **(a)** compressional wave velocity (V_p), **(b)** density, **(c)** porosity, **(d)** permeability.

linear correlation ($R^2 = 0.99$, $n = 4$) between V_p and vitrinite reflectance for burial conditions following the hydrostatic gradient (absence of overpressure), and here referred to normally-compacted, can be drawn from the boreholes BO1.1 to BO4.0 (Fig. 4a), indicating a gradual progression of compaction and lithification due to tighter grain packing, cementation and consequently a reduction in porosity and permeability. However, the decrease in V_p between BO4.0 and BO5.0 is indicative of potential overpressure conditions in the latter. V_p values from location BO5.0 clearly fall out of the general, normal compaction trend. More evidence towards this end is also given by the development of

log and laboratory-derived density and porosity data. A decrease in bulk density accompanied by an increase in porosity and permeability can be observed in the Amaltheenton-Fm between boreholes BO4.0 and BO5.0 (BO5.1), although the Amaltheenton-Fm experienced an approximately 900 m larger max. burial depth at the BO5.0 site following the 3D modelling results published by Castro-Vera et al. (2024). These trends in the investigated parameters contradict the general trend of increasing density and compressional wave velocity with greater burial depth, while porosity increases. In fact, all investigated petrophysical properties for a thermal maturity range somewhere between 0.87 and 1.51 VRr %, or related maximum burial temperatures and depths of 127 to 163 °C, and 2440 to 3300 m (from Castro-Vera et al., 2024) deviate from trends expectable along gradual compaction and cementation.

5.4 Comparison of scale- and depth-dependent hydraulic behaviour

While petrophysical parameters such as density and porosity showed tight overlap between field and laboratory derived data, the hydraulic conductivity showed pronounced differences on both scales. Gautschi (2017) compiled hydraulic conductivity data derived from packer tests conducted at multiple locations within the Opalinuston Formation (OPA). These data, sourced from various studies, reveal a strong current depth dependency of hydraulic conductivity (Fig. 15). In the uppermost decametres, particularly from shallow boreholes in the Swabian Alb (Germany) and the Lausen borehole (Switzerland), decompaction and weathering exert a clear influence, resulting in elevated conductivity values as high as 10?4 $m\,s^{-1}$ near the surface (Hekel, 1994; Gautschi, 2017; Vogt et al., 2017). With increasing depth, the values decrease rapidly by several orders of magnitude, reaching as low as $10^{-13}\,m\,s^{-1}$ below 28 m (Vogt et al., 2017). As overburden increases, the rate of this decline vanishes, as observed in the deeper boreholes Rinken and Benken (Gautschi, 2017; Vogt et al., 2017).

The hydraulic conductivities from the packer test series in boreholes BO1.0, BO2.0, BO3.1, and BO4.0 vary over two orders of magnitude. The lowest value, $1.15 \times 10^{-7}\,m\,s^{-1}$, was recorded in BO4.0 at a depth between 24.8 and 31.9 m, which is consistent with the values for the OPA compiled by Gautschi (2017). In contrast, the values from BO1.0, BO2.0, and BO3.1 are notably higher than those reported for comparable depths (> 63 m below ground level) in Gautschi's (2017) compilation. Hekel (1994) suggests that variations in local topography and geomorphological evolution may influence the thickness of the decompaction zone, potentially accounting for the higher hydraulic conductivities observed in BO1.0, BO2.0, and BO3.1.

Hydraulic conductivities derived from unconfined pycnometer tests on intact specimens taken from cores across the decompaction zone of boreholes BO1 to BO5 range

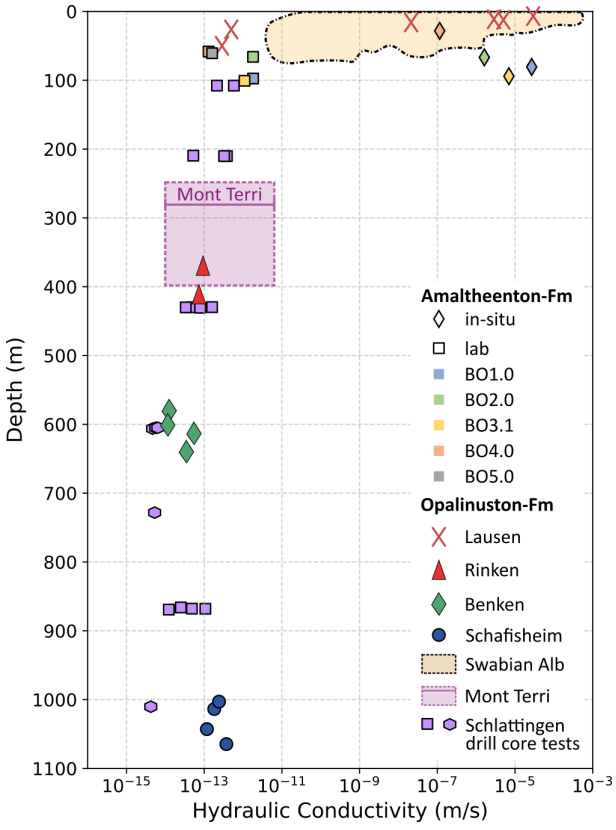

Figure 15. Hydraulic conductivity vs. depth plot of the Opalinuston-Fm from boreholes in Northern Switzerland (Lausen, Rinken, Benken, Schafisheim, Schlattringen), the Mont Terri underground research lab, and the Swabian Alb (Germany) derived from packer tests and confined permeability measurements on core specimens (adapted from: Gautschi, 2017) supplemented by lab and in-situ values of the Amaltheenton-Fm from borehole locations BO1-BO4. For data references of the individual boreholes, see Gautschi (2017).

from 0.15×10 to $1.91 \times 10^{-12}\,m\,s^{-1}$, seven orders of magnitude lower than the rock mass hydraulic conductivity at similar depth. Similar observations were made by Crisci et al., (2019) in the shallow Lausen borehole that penetrated the Opalinuston-Fm. While laboratory derived hydraulic conductivity continuously falls in a range between 10^{-14} to $10^{-12}\,m\,s^{-1}$ (in dependence on effective confining pressure during testing) along the whole borehole, in-situ data from packer tests lies several orders of magnitude above these values. However, in Lausen in-situ hydraulic conductivities showed a rapid decay with depth and below 30 m depth largely coincide with laboratory derived values (Crisci et al., 2019). Notably, the hydraulic conductivities of intact core specimens from the decompaction zone largely coincide with those obtained from packer tests and intact core specimens from deeper boreholes, below the decompaction zone (Fig. 15). The intact rock matrix, represented by laboratory experiments, retains low permeability characteristics

as a result of past maximum burial depth and associated compaction. In contrast, the rock mass hydraulic characteristics are strongly dependent on the present-day depth, as indicated by enhanced, fracture dominated hydraulic conductivity across the decompaction zone. This results in a pronounced lab-to-field contrast at shallow depths. The discrepancy between intact rock and rock mass hydraulic conductivity gradually vanishes with increasing depth. The observed decrease in rock mass hydraulic conductivity with depth, where the rock mass hydraulic properties approach those of intact rock specimens, may be attributed to fracture closure (Vogt et al., 2017; Crisci et al., 2019). These considerations deduced from the made observations remain preliminary and are currently assessed in an individual study in the framework of the MATURITY project.

6 Conclusion

The MATURITY project aims to investigate systematic changes in physical and chemical rock properties such as porosity, density, permeability, elasticity, CEC, and reactive surface area related to the variable burial history of the Upper Pliensbachian Amaltheenton-Fm in Lower Saxony (Germany). By analyzing observed correlations, the project aims to deepen our understanding of how these key properties evolve with gradual burial, thereby enhancing the transferability of geoscientific data for the site selection of clay-rich formations as potential host rocks for high-level radioactive waste repositories.

For this purpose, eight boreholes at five locations were drilled in the Hils- and Sack Syncline area, which is part of the southwestern margin of the Lower Saxony Basin. In this contribution, we present first results and insights into formation characteristics that were evaluated based on drill core material and in-situ investigations. The investigated parameters comprise the bulk mineralogical composition of the Amaltheenton-Fm, elemental ratios of Th, K, and U from spectral gamma-ray logs, compressional wave velocities (from FWS logs), bulk density and porosity (from Hepycnometry and GGD logging), permeability, and hydraulic conductivity (inferred from laboratory-based permeability experiments and in-situ packer tests). The increase in thermal maturity is documented by several parameters (VRr, TOC, HI, T_{max}).

We demonstrate that the bulk mineralogical composition of the Amaltheenton-Fm can be classified across the area of investigation and through a thickness of at least 94 m as argillaceous, with a consistent clay mineral content exceeding 58 % and a dominance in mixed-layer clay assemblage. The bulk mineral compositions are similar to those of the Jurensismergel-Fm/Opalinuston-Fm in the hanging wall. Thermal maturity increases from the southeastern to the northwestern part of the study area. This trend could be confirmed based on different parameters, including vitrinite reflectance (VRr ranging between 0.48 and 1.51 VRr %), and is inferred to be induced by variable maximum depth reached during the burial history. Both findings are vital for the MATURITY project and highlight the suitability of the Amaltheenton-Fm for the stated objectives.

Compressional wave velocity, bulk density, porosity, and permeability derived from laboratory experiments and in-situ methods yield a systematic correlation across a thermal maturity range between 0.48 and 0.87 VRr %, corresponding to burial depths between 1400 and 2440 m (burial depth from Castro-Vera et al., 2024). A deviation from this trend (see Fig. 14) is observed at higher thermal maturities between 0.87 and 1.51 VRr %, or related burial depths between 2440 and 3300 m, for all of these properties (burial depth from Castro-Vera et al., 2024). Assuming that the maturity sequence reflects variations in maximum burial temperatures, significant changes in different physical properties of the Amaltheenton-Fm such as porosity, density, and compressional wave velocity, occur within an empirically derived temperature range between 124 and 169 °C. These changes contradict expected normal compaction trends (Fig. 16). The observations align with previous studies (Gaus et al., 2022; Castro-Vera et al., 2024) which attribute the divergence of measured parameters at burial depths greater than 2440 m to overpressure generation and migration within the overlaying Posidonienschiefer-Fm during gas generation. It is important to emphasize that these deviations illustrate the site-specific nature of burial-related property trends. Local processes such as overpressure generation, hydrochemical evolution, or changes in effective stress can modify or even invert depth-dependent trends. Consequently, burial-related trends in individual material properties should not be interpreted as a direct proxy for host-rock suitability, as repository-relevant material behaviour emerges from the mutual interaction of these properties with site-specific boundary conditions such as stress state, hydrochemistry, and structural overprint. In this sense, the presented burial trends provide process-based constraints on property evolution that can support data transfer to sites with limited property information, but they do not constitute a standalone criterion for evaluating or comparing repository sites. First hydraulic double-packer tests in four boreholes (BO1.0, BO2.0, BO3.1, and BO4.0) delivered hydraulic conductivity ranges spanning several orders of magnitude. The measurements suggest hydrogeological conditions dominated by decompaction effects such as fracturing, that are traceable to depths of 100 m. As a result, the rock mass scale (metre to decametre), does not yield correlations between the maximum burial depth and the hydraulic properties. In contrast, based on a comparison with hydraulic data of the Opalinuston-Fm, the distribution of hydraulic conductivity rather suggests a dependency of present-day depth (Gautschi, 2017; Vogt et al., 2017; Crisci et al., 2019). However, changes in hydraulic transport properties with burial depth can generally be expected in the intact rock, as evidenced by laboratory gas permeability data from all bore-

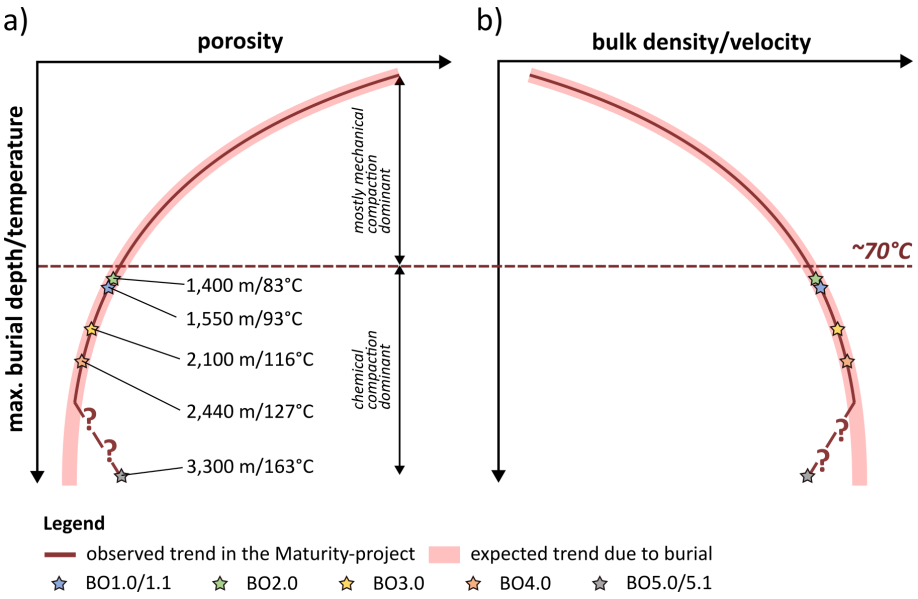

Figure 16. Simplified depiction of expected and observed alterations in **(a)** porosity and **(b)** density and compressional wave velocity induced by changing stress and temperature conditions during burial. Observed changes in properties follow the generally expected trends during burial for a thermal maturity range between 0.48 and 0.87 VRr % (BO1.0 to BO4.0) or related temperatures between 83 and 127 °C. A deviation for the same properties from the generally expected trend was observed for a thermal maturity of 1.51 VRr % (BO5.0) or a related maximum burial temperature of 163 °C. The dashed horizontal line at ∼ 70 °C marks the approximate onset of illite–smectite transformation and the shift from mechanically to chemically dominated diagenesis (Bjørlykke, 1998; Peltonen et al., 2009). Temperature and property ranges are not to scale. Burial depth and temperatures after Castro-Vera et al. (2024).

hole locations. An initial decrease in permeability follows the thermal maturity increase between 0.48 and 0.87 VRr %. For a thermal maturity of 1.51 VRr % a slight increase in permeability was observed. Collectively, these observations suggest that the intact rock hydraulic behavior remains largely unaltered after uplift and reflects past maximum burial. In contrast, in the decompaction zone, this low permeable matrix is superimposed by fractures on the rock mass scale.

Currently, individual studies carried out in the framework of the MATURITY project aim to further investigate the complex dependencies and interactions between burial history and mineralogical (CEC and reactive surface area), petrophysical (porosity, permeability), mechanical (rock strength and elasticity), and hydrogeological (hydraulic conductivity, storativity) claystone properties. These detailed studies will complement the previous analyses to deliver an important data set for the further site selection process in Germany. Ultimately, this effort will (a) enhance the understanding of the processes altering claystone properties throughout their burial and uplift and (b) facilitate robust site and scale data transferability by establishing transfer functions for the investigated parameters.

Data availability. Most data generated and analysed in this study are presented directly in the tables and figures of this article. The underlying datasets supporting the figures and analyses are available at: https://doi.org/10.5281/zenodo.18849751 (Burchartz and Seemann, 2026).

Author contributions. RB, TS, GG, LW, MRJ, BMM, SG, RL, FA, LB, MCC: investigation. RB, RL: writing (original draft preparation). RB: visualization. LW, TS, GG, MRJ, RB, SG, FA, RL, JE, BMM, LB, MCC: writing (review and editing). FA, RL, JE:yconceptualization, funding acquisition. FA, RL: supervision.

Competing interests. The contact author has declared that none of the authors has any competing interests.

Disclaimer. Publisher's note: Copernicus Publications remains neutral with regard to jurisdictional claims made in the text, published maps, institutional affiliations, or any other geographical representation in this paper. The authors bear the ultimate responsibility for providing appropriate place names. Views expressed in the text are those of the authors and do not necessarily reflect the views of the publisher.

Acknowledgements. This project received funding from the Federal Company for Radioactive Waste Disposal and the Federal Ministry for Economic Affairs and Climate Action, which is greatly acknowledged. We gratefully acknowledge the insightful and constructive comments provided by Dr. Daniel Minisini and Dr. Ben

Laurich. Their careful revision and thoughtful suggestions substantially strengthened the manuscript.

Financial support. This project received funding from the Federal Company for Radioactive Waste Disposal and the Federal Ministry for Economic Affairs and Climate Action.

This open-access publication was funded by the RWTH Aachen University.

Review statement. This paper was edited by Kei Ogata and reviewed by Daniel Minisini and Ben Laurich.

References

Adams, J. A. S. and Weaver, C. E.: Thorium-to-Uranium Ratios as Indicators of Sedimentary Processes: Example of Concept of Geochemical Facies, AAPG Bull., 42, 387–430, 1958.

Addis, M. A. and Jones, M. E.: Volume changes during diagenesis, Mar. Petrol. Geol., 2, 241–246, https://doi.org/10.1016/0264-8172(85)90013-3, 1985.

Adriasola Muñoz, Y.: The thermal history of the Western Lower Saxony Basin, Germany, 1. Aufl., Verlagshaus Mainy GmbH Aachen, Mainz, Aachen, 152 pp., ISBN 3-86130-884-3, 2007.

Amann, F., Wild, K. M., Loew, S., Yong, S., Thoeny, R., and Frank, E.: Geomechanical behaviour of Opalinus Clay at multiple scales: results from Mont Terri rock laboratory (Switzerland), Swiss J. Geosci., 110, 151–171, https://doi.org/10.1007/s00015-016-0245-0, 2017.

Aplin, A. C. and Macquaker, J. H. S.: Mudstone diversity: Origin and implications for source, seal, and reservoir properties in petroleum systems, AAPG Bull., 95, 2031–2059, https://doi.org/10.1306/03281110162, 2011.

Aplin, A. C. and Yang, Y.: Assessment of ß, the compression coefficient of mudstones and its relationship with detailed lithology, Mar. Petrol. Geol., 12, 955–963, 1995.

Aplin, A. C., Matenaar, I. F., McCarty, D. K., and Van Der Pluijm, B. A.: Influence of Mechanical Compaction and Clay Mineral Diagenesis on the Microfabric and Pore-Scale Properties of Deep-Water Gulf of Mexico Mudstones, Clay. Clay Miner., 54, 500–514, https://doi.org/10.1346/CCMN.2006.0540411, 2006.

Armitage, P. J., Worden, R. H., Faulkner, D. R., Aplin, A. C., Butcher, A. R., and Iliffe, J.: Diagenetic and sedimentary controls on porosity in Lower Carboniferous fine-grained lithologies, Krechba field, Algeria: A petrological study of a caprock to a carbon capture site, Mar. Petrol. Geol., 27, 1395–1410, https://doi.org/10.1016/j.marpetgeo.2010.03.018, 2010.

Athy, L. F.: Density, Porosity and Compaction of Sedimentary Rocks, AAPG Bull., 14, 1–24, https://doi.org/10.1306/3D93289E-16B1-11D7-8645000102C1865D, 1930.

Bachmann, G. H., Voigt, T., Bayer, U., von Eynatten, H., Legler, B., Littke, R., Breitkreuz, Ch., Geiβler, M., Schneider, J., Kiersnowski, H., Stollhofen, H., Barnasch, J., Beutler, G., Franz, M., Kästner, M., Mutterlose, J., Radies, D., Reicherter, K., von Eynatten, H., Littke, R., Voigt, S., Kley, J., Sirocko, F., Lehné, R., Hübscher, Ch., Winsemann, J., and Stackebrandt, W.: Basin Fill, in: Dynamics of Complex Intracontinental Basins: The Central European Basin System, edited by: Littke, R., Bayer, U., Gajewski, D., and Nelskamp, S., Springer Berlin Heidelberg, Berlin, Heidelberg, 156–245, https://doi.org/10.1007/978-3-540-85085-4_4, 2008.

Baldschuhn, R. and Kockel, F.: Der Untergrund von Hannover und seiner Umgebung, Naturhistorische Gesellschaft Hannover, 1998.

Barker, C. E. and Pawlewicz, M. J.: Calculation of Vitrinite Reflectance from Thermal Histories and Peak Temperatures, in: Vitrinite Reflectance as a Maturity Parameter, vol. 570, American Chemical Society, 216–229, https://doi.org/10.1021/bk-1994-0570.ch014, 1994.

Bastiaens, W., Bernier, F., and Li, X. L.: SELFRAC: Experiments and conclusions on fracturing, self-healing and self-sealing processes in clays, Phys. Chem. Earth Pts. A/B/C, 32, 600–615, https://doi.org/10.1016/j.pce.2006.04.026, 2007.

Basu, S., Jones, A., and Mahzari, P.: Best Practices for Shale Core Handling: Transportation, Sampling and Storage for Conduction of Analyses, Journal of Marine Science Engineering, 8, 136, https://doi.org/10.3390/jmse8020136, 2020.

Bataller, F. J., McDougall, N. D., and Moscariello, A.: Reviewing the correlation potential of Spectral Gamma Ray: a case study in Ordovician glacial environments in the Murzuq basin, SW Libya, J. Afr. Earth Sci., 188, 104475, https://doi.org/10.1016/j.jafrearsci.2022.104475, 2022.

Bernard, S., Horsfield, B., Schulz, H.-M., Wirth, R., Schreiber, A., and Sherwood, N.: Geochemical evolution of organic-rich shales with increasing maturity: A STXM and TEM study of the Posidonia Shale (Lower Toarcian, northern Germany), Mar. Petrol. Geol., 31, 70–89, https://doi.org/10.1016/j.marpetgeo.2011.05.010, 2012.

Berthonneau, J., Hoover, C. G., Grauby, O., Baronnet, A., Pellenq, R. J.-M., and Ulm, F.-J.: Crystal-chemistry control of the mechanical properties of 2 : 1 clay minerals, Appl. Clay Sci., 143, 387–398, https://doi.org/10.1016/j.clay.2017.04.010, 2017.

Betz, D., Führer, F., Greiner, G., and Plein, E.: Evolution of the lower Saxony Basin, Tectonophysics, 137, 127–170, 1987.

BGE: Zwischenbericht Teilgebiete gemäß §13 StandAG, Bundesgesellschaft für Endlagerung, https://www.bge.de/fileadmin/user_upload/Standortsuche/ (last accessed: 10 June 2024), 2020.

Bjørlykke, K.: Clay mineral diagenesis in sedimentary basins – a key to the prediction of rock properties. Examples from the North Sea Basin, Clay Miner., 33, 15–34, 1998.

Bjørlykke, K.: Effects of compaction processes on stresses, faults, and fluid flow in sedimentary basins: examples from the Norwegian margin, Geol. Soc. Spec. Publ., 253, 359–379, https://doi.org/10.1144/GSL.SP.2006.253.01.19, 2006.

Bjørlykke, K. and Høeg, K.: Effects of burial diagenesis on stresses, compaction and fluid flow in sedimentary basins, Mar. Petrol. Geol., 14, 267–276, https://doi.org/10.1016/S0264-8172(96)00051-7, 1997.

Blümling, P., Bernier, F., Lebon, P., and Derek Martin, C.: The excavation damaged zone in clay formations time-dependent behaviour and influence on performance assessment, Phys. Chem. Earth Pts. A/B/C, 32, 588–599, https://doi.org/10.1016/j.pce.2006.04.034, 2007.

Bock, H., Dehandschutter, B., Martin, D. C., Haller, A. de, Mazurek, M., Skoczylas, F., and Davy, C. (Eds.): Self-sealing of fractures in argillaqceous formations in the context of geological disposal of radioactive waste: review and synthesis, OECD, Paris, 310 pp., OECD, ISBN 978-92-64-99095-1, 2010.

Bonin, B.: Deep geological disposal in argillaceous formations: studies at the Tournemire test site, J. Contam. Hydrol., 35, 315–330, https://doi.org/10.1016/S0169-7722(98)00132-6, 1998.

Bossart, P., Meier, P. M., Moeri, A., Trick, T., and Mayor, J.-C.: Geological and hydraulic characterisation of the excavation disturbed zone in the Opalinus Clay of the Mont Terri Rock Laboratory, Eng. Geol., 66, 19–38, https://doi.org/10.1016/S0013-7952(01)00140-5, 2002.

Bossart, P., Trick, T., Meier, P. M., and Mayor, J.-C.: Structural and hydrogeological characterisation of the excavation-disturbed zone in the Opalinus Clay (Mont Terri Project, Switzerland), Appl. Clay Sci., 26, 429–448, https://doi.org/10.1016/j.clay.2003.12.018, 2004.

Bowers, G. L.: Pore Pressure Estimation From Velocity Data: Accounting for Overpressure Mechanisms Besides Undercompaction, SPE Dril. Completion, 10, 89–95, https://doi.org/10.2118/27488-PA, 1995.

Broichhausen, H., Littke, R., and Hantschel, T.: Mudstone compaction and its influence on overpressure generation, elucidated by a 3D case study in the North Sea, Int. J. Earth Sci. (Geol. Rundsch.), 94, 956–978, https://doi.org/10.1007/s00531-005-0014-1, 2005.

Bruns, B., Di Primio, R., Berner, U., and Littke, R.: Petroleum system evolution in the inverted Lower Saxony Basin, northwest Germany: a 3D basin modeling study, Geofluids, 13, 246–271, https://doi.org/10.1111/gfl.12016, 2013.

Bruns, B., Littke, R., Gasparik, M., Van Wees, J. -D., and Nelskamp, S.: Thermal evolution and shale gas potential estimation of the Wealden and Posidonia Shale in NW-Germany and the Netherlands: a 3D basin modelling study, Basin Res., 28, 2–33, https://doi.org/10.1111/bre.12096, 2016.

Burnaz, L., Littke, R., Grohmann, S., Erbacher, J., Strauss, H., and Amann, F.: Lower Jurassic (Pliensbachian–Toarcian) marine paleoenvironment in Western Europe: sedimentology, geochemistry and organic petrology of the wells Mainzholzen and Wickensen, Hils Syncline, Lower Saxony Basin, Int. J. Earth Sci. (Geol. Rundsch.), https://doi.org/10.1007/s00531-023-02381-8, 2024.

Busch, A., Schweinar, K., Kampman, N., Coorn, A., Pipich, V., Feoktystov, A., Leu, L., Amann-Hildenbrand, A., and Bertier, P.: Determining the porosity of mudrocks using methodological pluralism, Geol. Soc. Spec. Publ., 454, 15–38, https://doi.org/10.1144/SP454.1, 2017.

Burchartz, R. and Seemann, T.: MATURITY Project Data, Zenodo [data set], https://doi.org/10.5281/ZENODO.18849751, 2026.

Carcione, J. M., Gei, D., Yu, T., and Ba, J.: Effect of Clay and Mineralogy on Permeability, Pure Appl. Geophys., 176, 2581–2594, https://doi.org/10.1007/s00024-019-02117-3, 2019.

Castro-Vera, L., Amberg, S., Gaus, G., Leu, K., and Littke, R.: 3D basin modeling of the Hils Syncline, Germany: reconstruction of burial and thermal history and implications for petrophysical properties of potential Mesozoic shale host rocks for nuclear waste storage, Int. J. Earth Sci. (Geol. Rundsch.), https://doi.org/10.1007/s00531-024-02384-z, 2024.

Corkum, A. G. and Martin, C. D.: The mechanical behaviour of weak mudstone (Opalinus Clay) at low stresses, Int. J. Rock Mech. Min., 44, 196–209, https://doi.org/10.1016/j.ijrmms.2006.06.004, 2007.

Crank, J.: The mathematics of diffusion, 2d edn., Clarendon Press, Oxford, (Eng), 414 pp., ISBN 978-0-19-853344-3, 1975.

Cripps, J. C. and Czerewko, M. A.: The influence of diagenetic and mineralogical factors on the breakdown and geotechnical properties of mudrocks, Geol. Soc. Spec. Publ., 454, 271–293, https://doi.org/10.1144/SP454.10, 2017.

Crisci, E., Ferrari, A., Giger, S. B., and Laloui, L.: Hydro-mechanical behaviour of shallow Opalinus Clay shale, Eng. Geol., 251, 214–227, https://doi.org/10.1016/j.enggeo.2019.01.016, 2019.

Czerewko, M. A. and Cripps, J. C.: The implications of diagenetic history and weathering on the engineering behaviour of mudrocks, in: IAEG2006, 10th Congress of the International Association for Engineering Geology and the Environment, Nottingham, UK, 6–10 September 2006, 2006.

Delage, P., Cui, Y. J., and Tang, A. M.: Clays in radioactive waste disposal, Journal of Rock Mechanics and Geotechnical Engineering, 2, 111–123, https://doi.org/10.3724/SP.J.1235.2010.00111, 2010.

Dewhurst, D. N., Aplin, A. C., Sarda, J., and Yang, Y.: Compaction-driven evolution of porosity and permeability in natural mudstones: An experimental study, J. Geophys. Res., 103, 651–661, https://doi.org/10.1029/97JB02540, 1998.

Dewhurst, D. N., Aplin, A. C., and Sarda, J.: Influence of clay fraction on pore-scale properties and hydraulic conductivity of experimentally compacted mudstones, J. Geophys. Res., 104, 29261–29274, https://doi.org/10.1029/1999JB900276, 1999.

Doebelin, N. and Kleeberg, R.: Profex: a graphical user interface for the Rietveld refinement program BGMN, J. Appl. Crystallogr., 48, 1573–1580, https://doi.org/10.1107/S1600576715014685, 2015.

Eaton, B. A.: The Equation for Geopressure Prediction from Well Logs, Fall Meeting of the Society of Petroleum Engineers of AIME: Society of Petroleum Engineers, https://doi.org/10.2118/5544-MS, 1975.

Ewy, R., Dirkzwager, J., and Bovberg, C.: Claystone porosity and mechanical behavior vs. geologic burial stress, Mar. Petrol. Geol., 121, 104563, https://doi.org/10.1016/j.marpetgeo.2020.104563, 2020.

Ewy, R. T.: Shale/claystone response to air and liquid exposure, and implications for handling, sampling and testing, Int. J. Rock Mech. Min., 80, 388–401, https://doi.org/10.1016/j.ijrmms.2015.10.009, 2015.

Fertl, W. H. and Chilingarian, G. V.: Type and distribution modes of clay minerals from well logging data, J. Petrol. Sci. Eng., 3, 321–332, https://doi.org/10.1016/0920-4105(90)90052-5, 1990.

Fink, R., Frohn, V., Froidl, F., Littke, R., and Uffmann, A. K.: Impact of burial history on petrophysical properties of Jurassic and Lower Cretaceous mudstones as potential nuclear waste storage sites in the Lower Saxony Basin, Northern Germany, Z. Dtsch. Ges. Geowiss., 170, 339–355, https://doi.org/10.1127/zdgg/2019/0191, 2019.

Fisher, Q., Kaminskaite, I., and Del Pino Sanchez, A.: Shale barrier performance in petroleum systems: implications for CO_2 storage

and nuclear waste disposal, Geoenergy, 1, geoenergy2023-006, https://doi.org/10.1144/geoenergy2023-006, 2023.

Gama, J. and Schwark, L.: Lithofacies of early Jurassic successions derived from spectral gamma ray logging in the Mandawa Basin, SE Tanzania, Arab. J. Geosci., 15, 1373, https://doi.org/10.1007/s12517-022-10622-4, 2022.

Gasparik, M., Bertier, P., Gensterblum, Y., Ghanizadeh, A., Krooss, B. M., and Littke, R.: Geological controls on the methane storage capacity in organic-rich shales, Int. J. Coal Geol., 123, 34–51, https://doi.org/10.1016/j.coal.2013.06.010, 2014.

Gaus, G., Amann-Hildenbrand, A., Krooss, B. M., and Fink, R.: Gas permeability tests on core plugs from unconventional reservoir rocks under controlled stress: A comparison of different transient methods, J. Nat. Gas Sci. Eng., 65, 224–236, https://doi.org/10.1016/j.jngse.2019.03.003, 2019.

Gaus, G., Hoyer, E.-M., Seemann, T., Fink, R., Amann, F., and Littke, R.: Laboratory investigation of permeability, pore space and unconfined compressive strength of uplifted Jurassic mudstones: The role of burial depth and thermal maturation, Z. Dtsch. Ges. Geowiss., 173, 469–489, https://doi.org/10.1127/zdgg/2022/0329, 2022.

Gautschi, A.: Safety-relevant hydrogeological properties of the claystone barrier of a Swiss radioactive waste repository: An evaluation using multiple lines of evidence, Grundwasser, 22, 221–233, https://doi.org/10.1007/s00767-017-0364-1, 2017.

Ghanizadeh, A., Amann-Hildenbrand, A., Gasparik, M., Gensterblum, Y., Krooss, B. M., and Littke, R.: Experimental study of fluid transport processes in the matrix system of the European organic-rich shales: II. Posidonia Shale (Lower Toarcian, northern Germany), Int. J. Coal Geol., 123, 20–33, https://doi.org/10.1016/j.coal.2013.06.009, 2014.

Grathoff, G. H., Peltz, M., Enzmann, F., and Kaufhold, S.: Porosity and permeability determination of organic-rich Posidonia shales based on 3-D analyses by FIB-SEM microscopy, Solid Earth, 7, 1145–1156, https://doi.org/10.5194/se-7-1145-2016, 2016.

Grohmann, S., Littke, R., Abu-Mahfouz, I., Gaus, G., Klaver, J., Thüns, N., Schulte, P., Patzek, T., and Vahrenkamp, V.: The deposition of type II-S Jordan oil shale in the context of Late Cretaceous source rock formation in the Eastern Mediterranean realm. Insights from organic and inorganic geochemistry and petrography, Mar. Petrol. Geol., 148, 106058, https://doi.org/10.1016/j.marpetgeo.2022.106058, 2023.

Guglielmi, Y., Cappa, F., Shadoan, T., Ajo-Franklin, J., Soom, F., Lanyon, B., Cook, P., Hopp, C., Rodríguez Tribaldos, V., Robertson, M., Wood, T., Ulrich, C., Schefer, S., Nussbaum, C., and Birkholzer, J.: Control Mechanisms for Self-Sealing in Activated Clay-Rich Faults Through Controlled Hydraulic Injection Experiment, Water Resour. Res., 61, e2024WR037595, https://doi.org/10.1029/2024WR037595, 2025.

Hart, B. S., Schieber, J., and Kalinec, J.: Clay diagenesis and overpressure development in Upper Cretaceous and Tertiary shales of South Texas, Mar. Petrol. Geol., 147, 105978, https://doi.org/10.1016/j.marpetgeo.2022.105978, 2023.

Hekel, U.: Hydrogeologische Erkundung toniger Festgesteine am Beispiel des Opalinustons (Unteres Aalenium), Ph.D. thesis, Universität Tübingen, Tübingen, Germany, 170 pp., 1994.

Heunisch, C., Caspers, G., Elbracht, J., Langer, A., Röhling, H.-G., Schwarz, C., and Streif, H.: Erdgeschichte von Niedersachsen: Geologie und Landschaftsentwicklung, Landesamt für Bergbau, Energie und Geologie, Hannover, https://doi.org/10.48476/GEOBER_6_2017, 2018.

Hooker, J. N., Ruhl, M., Dickson, A. J., Hansen, L. N., Idiz, E., Hesselbo, S. P., and Cartwright, J.: Shale Anisotropy and Natural Hydraulic Fracture Propagation: An Example from the Jurassic (Toarcian) Posidonienschiefer, Germany, J. Geophys. Res.-Sol. Ea., 125, e2019JB018442, https://doi.org/10.1029/2019JB018442, 2020.

Ibanez, W. D. and Kronenberg, A. K.: Experimental deformation of shale: Mechanical properties and microstructural indicators of mechanisms, Int. J. Rock Mech. Min. and Geomechanics Abstracts, 30, 723–734, https://doi.org/10.1016/0148-9062(93)90014-5, 1993.

Jones, M. E. and Addis, M. A.: Volume change during sediment diagenesis and the development of growth faults, Mar. Petrol. Geol., 1, 118–122, https://doi.org/10.1016/0264-8172(84)90081-3, 1984.

Jones, M. E. and Addis, M. A.: On changes in porosity and volume during burial of argillaceous sediments, Mar. Petrol. Geol., 2, 247–253, https://doi.org/10.1016/0264-8172(85)90014-5, 1985.

Jordan, H.: Geologische Wanderkarte Leinebergland 1 : 100000, Niedersächsisches Landesamt für Bodenforschung, Hannover, 1989.

Khajooie, S., Gaus, G., Seemann, T., Ahrens, B., Hua, T., and Littke, R.: Exploring Effective Diffusion Coefficients in Water-Saturated Reservoir Rocks via the Pressure Decay Technique: Implications for Underground Hydrogen Storage, Transport Porous Med., 152, 12, https://doi.org/10.1007/s11242-024-02148-y, 2025.

Klaja, J. and Dudek, L.: Geological interpretation of spectral gamma ray (SGR) logging in selected boreholes, Nafta-Gaz, 72, 3–14, https://doi.org/10.18668/NG2016.01.01, 2016.

Klaver, J., Desbois, G., Urai, J. L., and Littke, R.: BIB-SEM study of the pore space morphology in early mature Posidonia Shale from the Hils area, Germany, Int. J. Coal Geol., 103, 12–25, https://doi.org/10.1016/j.coal.2012.06.012, 2012.

Koch, G. and Arnemann, H.: Die Inkohlung in Gesteinen des Rhät und Lias im südlichen Nordwestdeutschland, in: Geologisches Jahrbuch, vol. A29, Schweizerbart'sche Verlagsbuchhandlung, Hannover, 45–55, ISBN 978-3-510-96464-2, 1975.

Kockel, F., Wehner, H., and Gerling, P.: Petroleum Systems of the Lower Saxony Basin, Germany, in: The Petroleum System – From Source to Trap, vol. 60, edited by: Magoon, L. B. and Dow, W. G., American Association of Petroleum Geologists, https://doi.org/10.1306/M60585C34, 1994.

Lazar, O. R., Bohacs, K. M., Macquaker, J. H. S., Schieber, J., and Demko, T. M.: Capturing Key Attributes of Fine-Grained Sedimentary Rocks In Outcrops, Cores, and Thin Sections: Nomenclature and Description Guidelines, J. Sedimentary Res., 85, 230–246, https://doi.org/10.2110/jsr.2015.11, 2015.

Lehocki, I. and Avseth, P.: From cradle to grave: how burial history controls the rock-physics properties of quartzose sandstones, Geophys. Prospect., 69, 629–649, https://doi.org/10.1111/1365-2478.13039, 2021.

Li, Z., Dong, M., Li, S., and Dai, L.: A New Method for Gas Effective Diffusion Coefficient Measurement in Water-Saturated Porous Rocks under High Pressures, J. Porous Media, 9, 445–461, 2006.

Littke, R. and Rullkötter, J.: Mikroskopische und makroskopische Unterschiede zwischen Profilen unreifen und reifen Posidonienschiefers aus der Hilsmulde, Facies, 17, 171–179, https://doi.org/10.1007/BF02536781, 1987.

Littke, R., Baker, D. R., and Leythaeuser, D.: Microscopic and sedimentologic evidence for the generation and migration of hydrocarbons in Toarcian source rocks of different maturities, Advances in Organic Geochemistry, 13, 549–559, 1988.

Littke, R., Leythaeuser, D., Rullkötter, J., and Baker, D. R.: Keys to the depositional history of the Posidonia Shale (Toarcian) in the Hils Syncline, northern Germany, Geol. Soc. Spec. Publ., 58, 311–333, https://doi.org/10.1144/GSL.SP.1991.058.01.20, 1991.

Ma, X. and Zoback, M. D.: Static and Dynamic Response of Bakken Cores to Cyclic Hydrostatic Loading, Rock Mech. Rock Eng., 51, 1943–1953, https://doi.org/10.1007/s00603-018-1443-z, 2018.

Mackenzie, A. S., Leythaeuser, D., Altebäumer, F., Disko, U., and Rullkötter, J.: Molecular measurements of maturity for Lias δ shales in N. W. Germany, Geochim. Cosmoehim. Ac., 52, 1145–1154, 1988.

Mann, U.: Veränderung von Mineralmatrix und Porosität eines Erdölmuttergesteins durch einen Intrusivkörper (Lias epsilon 2–3: Hilsmulde, NW-Deutschland), 2. Tagung deutschsprachiger Sedimentologen, Heidelberg, 181–188, https://doi.org/10.1007/BF02536782, 1987.

Mann, U. and Müller, P. J.: Source rock evaluation by well log analysis (Lower Toarcian, Hils syncline), Advances in Organic Geochemistry, 13, 109–119, 1988.

Mathia, E. J., Bowen, L., Thomas, K. M., and Aplin, A. C.: Evolution of porosity and pore types in organic-rich, calcareous, Lower Toarcian Posidonia Shale, Mar. Petrol. Geol., 75, 117–139, https://doi.org/10.1016/j.marpetgeo.2016.04.009, 2016.

Maystrenko, Y., Bayer, U., Brink, H.-J., and Littke, R.: The Central European Basin System – an Overview, in: Dynamics of Complex Intracontinental Basins, edited by: Littke, R., Bayer, U., Gajewski, D., and Nelskamp, S., Springer Berlin Heidelberg, Berlin, Heidelberg, 16–34, https://doi.org/10.1007/978-3-540-85085-4_2, 2008.

Mazurek, M., Gautschi, A., Marschall, P., Vigneron, G., Lebon, P., and Delay, J.: Transferability of geoscientific information from various sources (study sites, underground rock laboratories, natural analogues) to support safety cases for radioactive waste repositories in argillaceous formations, Phys. Chem. Earth Pts. A/B/C, 33, S95–S105, https://doi.org/10.1016/j.pce.2008.10.046, 2008.

Mazurek, M., Wersin, P., Hadi, J., Grenèche, J.-M., Prinpreecha, N., and Traber, D.: Geochemistry and palaeo-hydrogeology of the weathered zone in the Opalinus Clay, Appl. Clay Sci., 232, 106793, https://doi.org/10.1016/j.clay.2022.106793, 2023.

Minisini, D., Simo, T., Macquaker, J. H. S., and Rudnicki, M. D.: Controls on storage capacity in mudstones. Cementation before sediment compaction and preservation of porosity in lithified rock, Mar. Petrol. Geol., 177, 107350, https://doi.org/10.1016/j.marpetgeo.2025.107350, 2025.

Mohnhoff, D., Littke, R., Krooss, B. M., and Weniger, P.: Flow-through extraction of oil and gas shales under controlled stress using organic solvents: Implications for organic matter-related porosity and permeability changes with thermal maturity, Int. J. Coal Geol., 157, 84–99, https://doi.org/10.1016/j.coal.2015.09.010, 2016.

Neuzil, C. E.: How permeable are clays and shales?, Water Resour. Res., 30, 145–150, https://doi.org/10.1029/93WR02930, 1994.

Neuzil, C. E.: Permeability of Clays and Shales, Annu. Rev. Earth Pl. Sc., 47, 247–273, https://doi.org/10.1146/annurev-earth-053018-060437, 2019.

NIBIS® Kartenserver: Geological map 1 : 25.000, Landesamt für Bergbau, Energie und Geologie (LBEG), Hannover, 2014.

Norris, S.: Radioactive waste confinement: clays in natural and engineered barriers – introduction, Geol. Soc. Spec. Publ., 443, 1–8, https://doi.org/10.1144/SP443.26, 2017.

OECD and NEA: Clay Club Catalogue of Characteristics of Argillaceous Rocks: 2022 Update, OECD, https://doi.org/10.1787/8860f7d8-en, 2022.

Ohazuruike, L. and Lee, K. J.: A comprehensive review on clay swelling and illitization of smectite in natural subsurface formations and engineered barrier systems, Nucl. Eng. Technol., 55, 1495–1506, https://doi.org/10.1016/j.net.2023.01.007, 2023.

Peltonen, C., Marcussen, Ø., Bjørlykke, K., and Jahren, J.: Clay mineral diagenesis and quartz cementation in mudstones: The effects of smectite to illite reaction on rock properties, Mar. Petrol. Geol., 26, 887–898, https://doi.org/10.1016/j.marpetgeo.2008.01.021, 2009.

Petmecky, S., Meier, L., Reiser, H., and Littke, R.: High thermal maturity in the Lower Saxony Basin: intrusion or deep burial?, Tectonophysics, 304, 317–344, https://doi.org/10.1016/S0040-1951(99)00030-X, 1999.

Pollastro, R. M.: Considerations and Applications of the Illite/Smectite Geothermometer in Hydrocarbon-Bearing Rocks of Miocene to Mississippian Age, Clay. Clay Miner., 41, 119–133, https://doi.org/10.1346/CCMN.1993.0410202, 1993.

Quirein, J. A., Gardner, J. S., and Watson, J. T.: Combined natural gamma ray spectral/litho-density measurements applied to complex lithologies, in: Soc. Pet. Eng. AIME, Pap., United States, Schlumberger Well Services, https://doi.org/10.2118/11143-MS, 1982.

Rider, M. H.: The geological interpretation of well logs, 2nd edn., revised, Rider-French Consulting, Sutherland, 280 pp., ISBN 0-9541906-0-2, 2000.

Roberts, R. M.: User's manual for nSIGHTS, Version 2.40 (p. 496), ERMS 544708, Sandia National Laboratories, Carlsbad, NM, 2006.

Rullkötter, J., Leythaeuser, D., Horsfield, B., Littke, R., Mann, U., Müller, P. J., Radke, M., Schaefer, R. G., Schenk, H.-J., Schwochau, K., Witte, E. G., and Welte, D. H.: Organic matter maturation under the influence of a deep intrusive heat source: A natural experiment for quantitation of hydrocarbon generation and expulsion from a petroleum source rock (Toarcian shale, northern Germany), Org. Geochem., 13, 847–856, https://doi.org/10.1016/0146-6380(88)90237-9, 1988.

Rutter, E., Mecklenburgh, J., and Taylor, K.: Geomechanical and petrophysical properties of mudrocks: introduction, Geol. Soc. Spec. Publ., 454, 1–13, https://doi.org/10.1144/SP454.16, 2017.

Rybacki, E., Reinicke, A., Meier, T., Makasi, M., and Dresen, G.: What controls the mechanical properties of shale rocks? – Part I: Strength and Young's modulus, J. Petrol. Sci. Eng., 135, 702–722, https://doi.org/10.1016/j.petrol.2015.10.028, 2015.

Schlumberger: Log Interpretation Charts, Schlumberger, Sugar Land, Texas, 293 pp., 2009.

Schmitz, H.-H.: Ölschiefer in Niedersachsen, Naturhistorische Gesellschaft Hannover, Hannover, 1980.

Senglaub, Y., Brix, M. R., Adriasola, A. C., and Littke, R.: New information on the thermal history of the southwestern Lower Saxony Basin, northern Germany, based on fission track analysis, Int. J. Earth Sci. (Geol. Rundsch.), 94, 876–896, https://doi.org/10.1007/s00531-005-0008-z, 2005.

Sone, H. and Zoback, M. D.: Mechanical properties of shale-gas reservoir rocks – Part 1: Static and dynamic elastic properties and anisotropy, Geophysics, 78, D381–D392, https://doi.org/10.1190/geo2013-0050.1, 2013.

Stahl, W. J.: Isotope geochemistry of light hydrocarbons adsorbed in Jurassic shales from the Hils syncline, North-west Germany, in: Abhandlungen der Braunschweigischen Wissenschaftlichen Gesellschaft, vol. 43, Erich Goltze KG, Göttingen, 103–125, ISBN 3-88452-225-6, 1992.

Stollhofen, H., Bachmann, G., Barnasch, J., Bayer, U., Beutler, G., Franz, M., Kästner, M., Legler, B., Mutterlose, J., and Radies, D.: Upper Rotliegend to Early Cretaceous basin development, in: Dynamics of complex intracontinental basins. The Central European Basin System, edited by: Littke, R., Bayer, U., Gajewski, D., and Nelskamp, S., Springer, Berlin, 181–210, https://link.springer.com/book/10.1007/978-3-540-85085-4, 2008.

Swarbrick, R. E. and Osborne, M. J.: Mechanisms that Generate Abnormal Pressures: An Overview, in: Abnormal Pressures in Hydrocarbon Environments, vol. 70, edited by: Law, B. E., Ulmishek, G. F., and Slavin, V. I., American Association of Petroleum Geologists, https://doi.org/10.1306/M70615C2, 1998.

Ufer, K. and Kleeberg, R.: Parametric Rietveld refinement of coexisting disordered clay minerals, Clay Miner., 50, 287–296, https://doi.org/10.1180/claymin.2015.050.3.03, 2015.

Ufer, K., Stanjek, H., Roth, G., Dohrmann, R., Kleeberg, R., and Kaufhold, S.: Quantitative phase analysis of bentonites by the rietveld method, Clay. Clay Miner., 56, 272–282, https://doi.org/10.1346/ccmn.2008.0560210, 2008.

Van Der Kamp, G.: Methods for determining the in situ hydraulic conductivity of shallow aquitards – an overview, Hydrogeol. J., 9, 5–16, https://doi.org/10.1007/s100400000118, 2001.

Van Wees, J.-D., Stephenson, R. A., Ziegler, P. A., Bayer, U., McCann, T., Dadlez, R., Gaupp, R., Narkiewicz, M., Bitzer, F., and Scheck, M.: On the origin of the Southern Permian Basin, Central Europe, Mar. Petrol. Geol., 17, 43–59, https://doi.org/10.1016/S0264-8172(99)00052-5, 2000.

Vogt, T., Hekel, U., Ebert, A., Becker, J. K., Traber, D., Giger, S., Brod, M., and Häring, C.: Hydrogeologische Untersuchungen im oberflächennahen Opalinuston (Bohrloch Lausen, Schweiz), Grundwasser, 22, 209–220, https://doi.org/10.1007/s00767-017-0363-2, 2017.

Voigt, T., Kley, J., and Voigt, S.: Dawn and dusk of Late Cretaceous basin inversion in central Europe, Solid Earth, 12, 1443–1471, https://doi.org/10.5194/se-12-1443-2021, 2021.

Wagner, J.-F.: Mechanical Properties of Clays and Clay Minerals, in: Developments in Clay Science, vol. 5, Elsevier, 347–381, https://doi.org/10.1016/B978-0-08-098258-8.00011-0, 2013.

Weaver, C. E. and Pollard, L. D.: The chemistry of clay minerals, Elsevier Scientific Pub. Co, Amsterdam New York, ISBN 0-444-41043-0, 1973.

Wiese, F. and Arp, G.: Ober-Jura und Ober-Kreide in Hils- und Sackmulde (NW-Deutschland) (Exkursion K am 5. April 2013) Upper Jurassic and Upper Cretaceous of the Hils and Sack Syncline (NW Germany), Jahresberichte und Mitteilungen des Oberrheinischen Geologischen Vereins, 95, 221–258, https://doi.org/10.1127/jmogv/95/2013/221, 2013.

Wijesinghe, P., Littke, R., Burnaz, L., Blumenberg, M., Erbacher, J., Mann, T., Amann, F., and Bauersachs, T.: Black shale deposition during the Early Jurassic: Geochemistry of Pliensbachian and Toarcian sedimentary rocks of the Hunzen Well, Hils Syncline, Northwest German Basin, The Depositional Record, 11, 1451–1478, https://doi.org/10.1002/dep2.70037, 2025.

Wild, K. M. and Amann, F.: Experimental study of the hydro-mechanical response of Opalinus Clay – Part 1: Pore pressure response and effective geomechanical properties under consideration of confinement and anisotropy, Eng. Geol., 237, 32–41, https://doi.org/10.1016/j.enggeo.2018.02.012, 2018a.

Wild, K. M. and Amann, F.: Experimental study of the hydro-mechanical response of Opalinus Clay – Part 2: Influence of the stress path on the pore pressure response, Eng. Geol., 237, 92–101, https://doi.org/10.1016/j.enggeo.2018.02.011, 2018b.

Winhausen, L., Khaledi, K., Jalali, M., Urai, J. L., and Amann, F.: Failure mode transition in Opalinus Clay: a hydro-mechanical and microstructural perspective, Solid Earth, 13, 901–915, https://doi.org/10.5194/se-13-901-2022, 2022.

Winhausen, L., Khaledi, K., Jalali, M., Bretthauer, M., and Amann, F.: The Anisotropic Behavior of a Clay Shale: Strength, Hydro-Mechanical Couplings and Failure Processes, J. Geophys. Res.-Sol. Ea., 128, e2023JB027382, https://doi.org/10.1029/2023JB027382, 2023.